CHAPTER 8

Analysis of interface cracks with contact in composites by 2D BEM

V. Mantič[1], A. Blázquez[2], E. Correa[1] & F. París[1]
[1]*Group of Elasticity and Strength of Materials, School of Engineering, University of Seville, Spain.*
[2]*Department of Mechanical Engineering, University of La Rioja, Spain.*

Abstract

Interfacial fracture mechanics covers a number of situations that at different levels characterize the appearance and growth of damage in Composites. The boundary element method (BEM) is well equipped to deal with situations where the variables of interest are associated to the boundary, fracture and contact mechanics being typical examples of these situations. This chapter is devoted to the application of interfacial fracture mechanics using BEM to characterize at different scales the damage in a fibrous composite material.

First, a review of the present situation of interfacial fracture mechanics including the two existing models (open model and contact model) that represent the stress state at the neighborhood of the crack tip is presented. The approaches based on the stress intensity factor (SIF) and the energy release rate (ERR) concepts are presented for isotropic and orthotropic materials. Special attention is devoted to the relation of the mode mixity measures that appear in the open model with the use of the two aforementioned approaches. A new expression for this relation is deduced and presented in this chapter. Then, the growth criteria (for crack propagation and kinking) derived from the SIF and ERR approaches are presented and discussed for both models.

Two applications at different levels of representation are analyzed. The first, at mesomechanical level of a composite, corresponds to the study of a delamination crack in a $[0_m, 90_n]_S$ laminate. The second, at micromechanical level of a composite, corresponds to an interface crack between fiber and matrix under a load transverse to the fiber. The growth of the debonding crack and its kinking into the matrix is studied.

1 Introduction: interface cracks in fiber reinforced composites

Fracture Mechanics applied to the study of cracks in isotropic homogeneous materials can be considered at present a well established area of knowledge (see, for instance, Andersson [3] and Janssen *et al*. [60]).

In contrast, Fracture Mechanics applied to interfacial cracks, a topic that has attracted an enormous research effort in recent years, is still a discipline under development. Since the pioneer work of Williams [145], England [32], Erdogan [34], Rice and Sih [113] and Malyshev and

WIT Transactions on State of the Art in Science and Engineering, Vol 21, © 2005 WIT Press
www.witpress.com, ISSN 1755-8336 (on-line)
doi:10.2495/978-1-85312-669-7/08

Salganik [75] among others, there have been significant contributions, the content of most of them being covered in Sections 2 and 3 of this chapter.

The development of Fracture Mechanics applied to interfacial cracks arises from the necessity of characterizing cracks of this type in different engineering applications, namely, the necessity of bonding metallic to composite components in the aeronautical industry, the characterization of internal damage (delamination) in composites or the use of layers of materials (recently of functionally graded materials) as thermal barrier coatings.

The applications considered in this chapter are associated to interface cracks that appear in composite materials characterizing mechanisms of damage at different levels. Thus, interface cracks between fibers and matrix at micro-mechanical level and delamination cracks between different layers at meso-mechanical level will be studied. There are many other possibilities of applications in the field of composites, such as the modeling of the fragmentation, pull-out, push-out or peeling tests.

Two Fracture Mechanics approaches have been developed for the analysis of interfacial cracks. One is called the open model and the other is called the contact model. In the open model the crack is assumed to be open whereas in the contact model the lips of the crack are assumed to come into contact at the two crack tips under the application of the load. The first approach is based on the works of Williams [145], Rice [112] and Hutchinson and Suo [56], among others, whereas the second is essentially based on the works of Comninou [19, 21], Comninou and Schmuesser [24] and Gautesen and Dundurs [40, 41].

Typically each approach has been applied to those cases where the coincidence of materials, geometry and loads made it more appropriate. There are however situations, see for instance the problem treated in París *et al*. [101] also treated here in Section 7, where both approaches can be used. To the knowledge of the authors there are many more publications based on the open model and in any case very few involving (either analytically, numerically or experimentally) both approaches.

The problems under consideration involve features (singular state of stresses at the boundary and contact along parts of the boundary) that make the boundary element method (BEM) the most suitable numerical method to deal with them. The three main characteristics of the use made of BEM in this study are Fracture Mechanics, Contact Mechanics and orthotropic behavior.

First in Sections 2 and 3 the background of the theory of interfacial cracks is presented. The proposals to deal with the two aforementioned models based on the stress intensity factor (SIF) and on the energy release rate (ERR) approaches are reviewed. A new relation between the mixity of the two fracture modes (I and II) in accordance with the two approaches mentioned is presented. The crack growth criteria associated to the two models considered and the two approaches followed are presented in Section 3.

A brief revision of the features of the BEM procedure here applied for isotropic and orthotropic materials is performed in Section 4. The features and solution procedure of the non linear contact problem is described in Section 5, with special emphasis on describing the application of contact conditions in a weak form.

Sections 6 and 7 present the two applications to composite materials already mentioned, the general conclusions being presented in Section 8.

2 Interface crack models

Consider two homogenous linearly elastic materials (denoted as 1 and 2), which are perfectly bonded along a surface except for a debonded region referred to as *interface crack*, subjected to

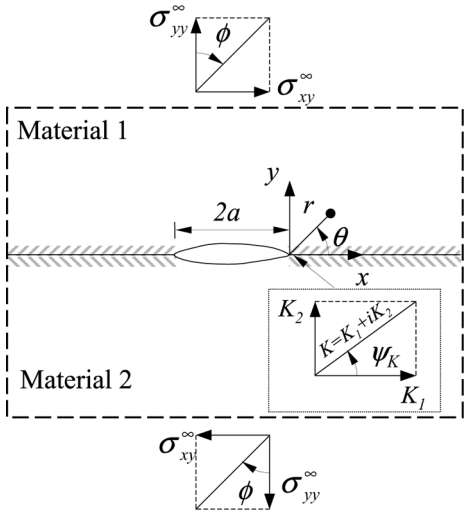

Figure 1: An interface crack problem configuration.

a far field loading, as in fig. 1. The interface between these materials is considered as a tough two-dimensional object without thickness. Tractions and displacements coincide at both sides of the bonded interface part whereas at the interface crack both materials may separate or maintain the contact, with or without relative sliding.

Referring to a fixed rectangular coordinate system (x, y, z), let σ_{ij} and u_i be the stresses and displacements in a linear elastic material. For the sake of simplicity, and also in view of the applications studied in Sections 6 and 7, theoretical explanations are in this work limited to plane situations. The analysis of anisotropic materials is restricted to orthotropic materials with symmetry planes coincident with the coordinate planes. Therefore, in-plane and out-of-plane solutions are decoupled, only in-plane stresses σ_{ij} $(i, j = x, y)$ being induced, but not σ_{iz} $(i = x, y)$, and the present work is only concerned with in-plane elastic solutions of interface crack problems.

In the *open model* of interface cracks, analyzed originally by Williams [145], the crack faces are supposed to be traction free in the same way as is usually supposed for cracks in homogeneous solids. An 'unexpected' basic aspect of the near-tip elastic solution of this model is that for a non-vanishing bimaterial mismatch parameter $\beta \neq 0$ (see definition for isotropic and orthotropic materials respectively in Sections 2.1 and 2.2) stresses and displacements start to oscillate when crack tip is approached. As a consequence of these displacement oscillations, an infinite number of regions where the crack faces interpenetrate and wrinkle is predicted by this solution (England [32], Erdogan [34]). The size of the zone where these physically non-admissible interpenetrations occur may be frequently very small, sometimes of atomic or subatomic scale. In view of this feature of the elastic solution in this open model, one would expect the existence of one or several contact zones in the vicinity of the interface crack tip.

In order to overcome the above inconsistencies of the open model, Comninou [19] developed the *contact model* of interface cracks. Proving that, allowing a frictionless contact between the crack faces, a physically correct solution with one (connected) contact zone at the crack tip is obtained when $\beta \neq 0$. Typically this contact zone extent is smaller than the size of the interpenetration zone in the open model, see París *et al*. [101] for a physical explanation of this relation, in a particular case.

Following an analysis by Rice [112], the actual behavior of an interface crack depends on the size of the zones of nonlinear material response (plasticity, nonlinear elastic deformations or other nonlinear effects) and/or contact. When this size is sufficiently small in comparison with the smallest characteristic length of the specimen (e.g. crack length or an adjacent layer thickness), then the open linear elastic model (Williams [145]) is adequate for interface crack growth predictions. The concept of *small-scale contact zone* (SSC) was introduced by Rice [112] to characterize such a situation with reference to a sufficiently small size of the near-tip contact zone.

However, if the above zones start to be physically relevant, being comparable to, or larger than, the smallest characteristic length of the specimen, other models including the phenomena which happen on a relevant scale, like linear elastic contact model (Comninou [19]), elasto-plastic (Shih and Asaro [117, 118]) or non-linear elastic (Knowles and Sternberg [63], Geubelle and Knauss [44]) models, should be applied.

In the present work, *small-scale yielding* (SSY) conditions (a basic concept of linear elastic fracture mechanics), with plasticity effects restricted to a sufficiently small zone, to characterize an interface crack growth by a linear elastic model, either open or with contact, will be assumed.

In this preliminary section some relevant properties of the near-tip singular elastic solutions associated to both, open and contact, models of interface cracks will be presented and discussed. Although a straight interface is considered here, it is believed that the basic conclusions given are applicable to the near-tip fields of curved interface cracks as well. The case of isotropic bimaterials will be analyzed first, and later some results dealing with generally orthotropic bimaterials will be introduced.

To complete the present review, the authors would like to recommend the following publications: a classical reference work on interfacial fracture mechanics by Hutchinson and Suo [56], a concise introduction to interface crack modeling in Hills *et al*. [54], and finally, a comprehensive review of the state of the art in interfacial fracture mechanics in the volume edited by Gerberich and Yang [42].

2.1 Isotropic bimaterials

Following Dundurs [31] the solution of a wide class of plane elastic problems for isotropic bimaterials depends only on two dimensionless mismatch parameters:

$$\alpha = \frac{G_1(\kappa_2 + 1) - G_2(\kappa_1 + 1)}{G_1(\kappa_2 + 1) + G_2(\kappa_1 + 1)} = \frac{E_1' - E_2'}{E_1' + E_2'}, \tag{1}$$

$$\beta = \frac{G_1(\kappa_2 - 1) - G_2(\kappa_1 - 1)}{G_1(\kappa_2 + 1) + G_2(\kappa_1 + 1)}, \tag{2}$$

where G_k is the shear modulus and κ_k the Kolosov's constant of material $k = 1, 2$. Let E_k and ν_k denote Young elasticity modulus and Poisson ratio respectively, then $G_k = E_k/2(1 + \nu_k)$. Effective elasticity modulus $E_k' = E_k/(1 - \nu_k^2)$ and $\kappa_k = 3 - 4\nu_k$ for plane strain, and $E_k' = E_k$ and $\kappa = (3 - \nu)/(1 + \nu)$ for plane stress state. α and β vanish for identical materials. In plane strain state, β is a measure for the mismatch in bulk moduli and vanishes for two incompressible materials or one incompressible and the other rigid.

Physically admissible values of mismatch parameters are restricted to a parallelogram in (α, β) plane enclosed by lines defined as $\alpha = \pm 1$, and by $\alpha = 4\beta \pm 1$ or $\alpha = (8\beta \pm 1)/3$ respectively in plane strain or plane stress state. Therefore, their ranges are $-1 \leq \alpha \leq 1$ and $-0.5 \leq \beta \leq 0.5$. Notice that, considering $\nu_1 \simeq \nu_2$, $\alpha, \beta > 0$ means that material 1 is stiffer than 2 and vice-versa for $\alpha, \beta < 0$.

2.1.1 Open model

According to Williams [145] asymptotic series expansion, near-tip singular tractions acting on the bonded part of an interface are approximated by:

$$(\sigma_{yy} + i\sigma_{xy})_{\theta=0} = (\sigma_{yy}^{\text{sing}} + i\sigma_{xy}^{\text{sing}})_{\theta=0} + O(1) = \frac{Kr^{i\varepsilon}}{\sqrt{2\pi r}} + O(1), \quad \text{for } r \to 0, \tag{3}$$

where r is the distance from the tip, $i = \sqrt{-1}$, ε is the oscillation index of the interface crack:

$$\varepsilon = \frac{1}{2\pi} \ln \frac{1-\beta}{1+\beta}, \tag{4}$$

$|\varepsilon| \leq (\ln 3)/2\pi \cong 0.175$, and $K = K_1 + iK_2$ is the complex SIF, which depends on the geometry and applied loading.

For $\beta = \varepsilon = 0$, solution in (3) is identical to that for a crack in a homogenous material and K_1 and K_2 coincide with the classical SIFs, K_{I} and K_{II}.

However, for $\varepsilon \neq 0$ SIF components K_1 and K_2 do not represent the opening and shear fracture modes respectively. Notice that the term $r^{i\varepsilon} = e^{i\varepsilon \ln r} = \cos(\varepsilon \ln r) + i \sin(\varepsilon \ln r)$ is responsible for the above mentioned oscillatory behavior (including sign changes) of each traction component superimposed over its well-known square root singular behavior when $r \to 0$. An implication of this oscillatory behavior in (3) is that, for $\varepsilon \neq 0$, infinite shear and normal (tensional and compressive) stresses are predicted at the crack tip independently of the character of the far-field load applied (tensile, shear or a combination of both). A consequence of these facts is that no separation of fracture modes, as for cracks in homogeneous solids, is possible here.

Nevertheless, it may be useful to observe that, multiplying expression in (3) by its conjugate, the sum of squares of normal and shear stresses obtained does not include any oscillatory term. This fact may be used in numerical solution of interface crack problems for an evaluation of the absolute value $|K|$ of the complex SIF.

The near-tip displacement jump across the crack $\Delta u_i(r) = u_i(r, \theta = \pi) - u_i(r, \theta = -\pi)$ is approximated by:

$$\begin{aligned} \Delta u_y + i\Delta u_x &= \Delta u_y^{\text{sing}} + i\Delta u_x^{\text{sing}} + O(r) \\ &= \frac{8}{1+2i\varepsilon} \frac{Kr^{i\varepsilon}}{\cosh(\pi\varepsilon)E^*} \sqrt{\frac{r}{2\pi}} + O(r), \quad \text{for } r \to 0, \end{aligned} \tag{5}$$

where

$$\frac{1}{E^*} = \frac{1}{2}\left(\frac{1}{E_1'} + \frac{1}{E_2'}\right) \tag{6}$$

is the average Young modulus, and $1/\cosh(\pi\varepsilon) = \sqrt{1-\beta^2}$. Multiplying the expression in (5) by its conjugate it is obtained that the magnitude of the displacement jump has no oscillatory term.

If the scale of perturbations of the theoretical linear elastic solution (like inelastic zone, contact zone, interface thickness and asperities) is sufficiently small in comparison with the smallest characteristic length of specimen r_g, given by the total crack length $2a$, thickness of an adjacent layer, etc., Williams singular oscillatory solution is approximately unperturbed in an annulus with the interior radius larger than the perturbation zone size but with the exterior radius smaller than r_g. Then, the elasticity field is completely characterized by the complex SIF K within this so-called K-annulus (Rice [112]).

As discussed in depth by Rice [112], K in (3) contains logarithms of length (which is a meaningless concept), its unit depends on ε and its phase angle depends on the length unit applied. Thus, it is suitable to introduce a reference length scale l defining a new complex SIF $\hat{K} = Kl^{i\varepsilon}$, which has the same units as the classical SIF in homogenous solids. Notice that $|\hat{K}| = |K|$. The choice of l is usually based either on the specimen geometry (crack length or layer thickness) or on a material scale (the plastic zone or fracture process zone).

Local phase angle $\psi_K = \arg \hat{K}$, defined through relation $\hat{K} = |\hat{K}|e^{i\psi_K}$, is an l-dependent measure of fracture mode mixity, $\tan \psi_K$ being equal to the relative proportion of shear to normal traction at the distance $r = l$ ahead of the crack tip. The following relation:

$$\tan\left(\psi_K + \varepsilon \ln \frac{r}{l}\right) = \frac{\mathrm{Im}[\hat{K}(r/l)^{i\varepsilon}]}{\mathrm{Re}[\hat{K}(r/l)^{i\varepsilon}]} = \frac{\sigma_{xy}^{\mathrm{sing}}}{\sigma_{yy}^{\mathrm{sing}}}(r, \theta = 0), \tag{7}$$

implies that the ratio $\sigma_{xy}^{\mathrm{sing}}/\sigma_{yy}^{\mathrm{sing}}$ varies periodically with $\ln(r/l)$ for $\varepsilon \neq 0$. In particular, what appears as a tensile field at a particular distance r to the crack tip will appear as a pure shear field at the distance $e^{-\pi/2\varepsilon}r$ or a pure compressive field at the other distance $e^{-\pi/\varepsilon}r$. Recall that this ratio is constant for cracks in bimaterials with $\varepsilon = 0$, as in homogeneous materials, where ψ_K reduces to the familiar mode mixity measure $\tan \psi_K = K_{\mathrm{II}}/K_{\mathrm{I}}$.

Local phase angles ψ_K and ψ'_K associated to two different reference lengths l and l' are related by equation

$$\psi'_K = \psi_K + \varepsilon \ln(l'/l). \tag{8}$$

Hence, the local phase angle shift between two choices of l in an interval of physically relevant scales may be negligible when ε is sufficiently small.

Note that the fracture mode mixity ψ_K may be nonzero when the far-field load phase angle ϕ defined in fig. 1 by $\tan \phi = \sigma_{xy}^{\infty}/\sigma_{yy}^{\infty}$ vanishes, i.e., when the load is perpendicular to the interface crack. Although ψ_K and ϕ are in general different, naturally there exists a strong correlation between them. In particular, the following relation (Rice [112]) holds for the case of two bonded half-spaces as in fig. 1: $\psi_K = \phi + \arctan(2\varepsilon) + \varepsilon \ln(l/2a)$.

As follows from the previous explanations, when $\varepsilon \neq 0$ then the reference length l should always be explicitly specified when ψ_K is used. Nevertheless, for the sake of simplicity l is usually tacitly omitted from expressions.

Expression (5) can be applied to determine regions where interpenetrations are predicted by the open model, Hills and Barber [53]. An estimation of the first interpenetration point defined by its distance from the crack tip r_i is obtained as the largest value of the expression

$$r_i = l \ \exp\left(((2n - \frac{1}{2})\pi - \psi_K + \arctan(2\varepsilon))/\varepsilon\right), \tag{9}$$

which is smaller than the crack length $2a$, n standing for an integer number.

In the particular case of two bonded half-spaces, it can be shown starting from (9) and assuming some tensile component of the far-field load, i.e. $-\frac{\pi}{2} < \phi < \frac{\pi}{2}$, and $\varepsilon > 0$, that $r_i = 2a \exp(-(\phi + \frac{\pi}{2})/\varepsilon)$ (Rice, 1988). Thus, r_i will be extremely small for ϕ near $\pi/2$, but it will not remain small for any $\varepsilon > 0$ when ϕ approaches $-\pi/2$.

Usually, following Rice [112], SSC conditions are associated to situations where the size of the interpenetration zone is less than 1% of the crack length, $r_i/2a < 0.01$. Hence, in the case of two bonded half-planes, SSC conditions are fulfilled when $\phi > -\pi/2 + 4.605\varepsilon$.

The singular oscillatory term in the asymptotic expansion of the near-tip stress and displacement field (cf. (3) and(5)) can be expressed in the form usually used for cracks in homogeneous

materials as:

$$\sigma_{ij}^{\text{sing}}(r,\theta) = \frac{1}{\sqrt{2\pi r}}\left(\text{Re}\left[\hat{K}(r/l)^{i\varepsilon}\right]\sigma_{ij}^{I}(\theta,\varepsilon) + \text{Im}\left[\hat{K}(r/l)^{i\varepsilon}\right]\sigma_{ij}^{\text{II}}(\theta,\varepsilon)\right), \quad -\pi \le \theta \le \pi, \tag{10}$$

$$u_i^{\text{sing}}(r,\theta) = \frac{1}{2G_k}\sqrt{\frac{r}{2\pi}}\left(\text{Re}\left[\hat{K}(r/l)^{i\varepsilon}\right]u_i^{I}(\theta,\varepsilon,\kappa_k) + \text{Im}\left[\hat{K}(r/l)^{i\varepsilon}\right]u_i^{\text{II}}(\theta,\varepsilon,\kappa_k)\right), \quad \theta_k^- \le \theta \le \theta_k^+, \tag{11}$$

where $\theta_k^- = 0, -\pi$, and $\theta_k^+ = \pi, 0$ $(k = 1, 2)$. Universal dimensionless functions σ_{ij}^m and u_i^m $(m = \text{I}, \text{II})$ were presented by Deng [26, 30] in cartesian coordinates. Rice *et al*. [114] presented expressions and plots of σ_{ij}^m in polar coordinates. A somewhat surprising feature of expression in (10) is that, when $\varepsilon = 0$ this expression reduces to the classical expression of near-tip stresses for cracks in homogeneous solids independently of α value.

With reference to the energy approach in interfacial fracture mechanics, the total strain ERR due to a crack extension along the interface (G^{int}) can be evaluated applying the classical virtual crack closure method, originally developed by Irwin [59] for cracks in homogeneous solids, to the near-tip elastic field of the open model as well. Consider first a small but finite crack extension Δa in Irwin's crack closure integrals. Then

$$G^{\text{int}}(\Delta a) = G_{\text{I}}^{\text{int}}(\Delta a) + G_{\text{II}}^{\text{int}}(\Delta a), \tag{12}$$

where

$$G_{\text{I}}^{\text{int}}(\Delta a) = \frac{1}{2\Delta a}\int_0^{\Delta a}\sigma_{yy}(r,0)\Delta u_y(\Delta a - r)dr, \tag{13}$$

$$G_{\text{II}}^{\text{int}}(\Delta a) = \frac{1}{2\Delta a}\int_0^{\Delta a}\sigma_{xy}(r,0)\Delta u_x(\Delta a - r)dr. \tag{14}$$

The total ERR $G^{\text{int}}(\Delta a)$ is converging (even being constant when only singular terms in (3) and (5) are considered) for $\Delta a \to 0$. Thus, the following limit exists:

$$G^{\text{int}} = \lim_{\Delta a \to 0} G^{\text{int}}(\Delta a). \tag{15}$$

The Irwin-type relation of the total strain ERR G^{int} in (15) in terms of the complex SIF was deduced by Malyshev and Salganik [75]:

$$G^{\text{int}} = \frac{|\hat{K}|^2}{\cosh^2(\pi\varepsilon)E^*} \tag{16}$$

This relation can be directly obtained by evaluation of the integral:

$$\frac{1}{2\Delta a}\int_0^{\Delta a}(\sigma_{yy}^{\text{sing}}(r,0) + i\sigma_{xy}^{\text{sing}}(r,0))(\Delta u_y^{\text{sing}}(\Delta a - r) - i\Delta u_x^{\text{sing}}(\Delta a - r))dr, \tag{17}$$

applying formula

$$\int_0^{\Delta a}\left(\frac{\Delta a - r}{r}\right)^{1/2 - i\varepsilon}dr = \frac{\pi\Delta a}{\cosh(\pi\varepsilon)}\left(\frac{1}{2} - i\varepsilon\right), \tag{18}$$

which implies that the imaginary part of (17) vanishes.

As can be seen G^{int} only depends, as in homogenous materials, on the magnitude of the complex SIF $\hat{K}$ and not on its phase angle ψ_K. The maximum value of G^{int} that an interface can sustain at a prescribed ψ_K without decohesion is called interface toughness at this fracture mode mixity denoted as $G_c^{\text{int}}(\psi_K)$.

In the following, the possibility of defining a fracture mode mixity measure based on the ERR concept will be shortly discussed. Due to the oscillatory character of the near-tip elastic field, $G_{\text{I}}^{\text{int}}(\Delta a)$ and $G_{\text{II}}^{\text{int}}(\Delta a)$ oscillate as well, and consequently their limits do not exist as $\Delta a \to 0$. This oscillatory behavior was studied by several authors, see Sun and Jih [124], Raju *et al.* [111] and Toya [138] among others. Mantič and París [82] recently deduced (developing a Toya's result, [138]) the following new explicit expressions of the individual components of the ERR associated to Δa, considering only singular terms in (3) and (5):

$$G_{\text{I,II}}(\Delta a) = 0.5G^{\text{int}}\left[1 \pm F(\varepsilon)\cos\left\{2(\psi_K + 2\psi_0(\Delta a/l, \varepsilon))\right\}\right], \tag{19}$$

where

$$2\psi_0(\Delta a/l, \varepsilon) = 2\varepsilon \ln(\Delta a/2l) + \varphi(\varepsilon) - \arctan(2\varepsilon), \tag{20}$$

$$F(\varepsilon) = \sqrt{\frac{\sinh(2\pi\varepsilon)}{2\pi\varepsilon(1+4\varepsilon^2)}} \quad \text{and} \quad \varphi(\varepsilon) = \arg\left[\frac{\Gamma(\frac{1}{2}+i\varepsilon)}{\Gamma(1+i\varepsilon)}\right], \tag{21}$$

$\Gamma(\cdot)$ being the gamma function. Basic features of the behavior of the amplitude function $F(\varepsilon)$ and phase angle shift function $\varphi(\varepsilon)$ are clearly seen from their Maclaurin series:

$$F(\varepsilon) = 1 + 1.289868\varepsilon^2 + O(\varepsilon^4) \quad \text{and} \quad \varphi(\varepsilon) = -2\varepsilon\ln 2 + 2.404114\varepsilon^3 + O(\varepsilon^5). \tag{22}$$

As follows from (19), the 'energetic' mode mixity $G_{\text{II}}^{\text{int}}/G_{\text{I}}^{\text{int}}$, frequently used in some applications for cracks in homogenous materials, cannot in general be unambiguously defined for interface cracks due to the oscillatory behavior of $G_{\text{I}}^{\text{int}}(\Delta a)$ and $G_{\text{II}}^{\text{int}}(\Delta a)$ with Δa. A consequence of these oscillations is that the phase angle ψ_G, an ERR based measure of the mode mixity, defined as:

$$\tan^2\psi_G = \frac{G_{\text{II}}^{\text{int}}(\Delta a)}{G_{\text{I}}^{\text{int}}(\Delta a)}, \quad 0 \le \psi_G \le \frac{\pi}{2}, \tag{23}$$

depends on Δa. Nevertheless, the fact that, for a very small ε, ψ_G is a weak function of Δa inside a physically relevant interval of Δa (in a similar way as ψ_K is a function of l), is used by some authors as a justification for application of the 'energetic' mode mixity to predict interface crack behavior.

Starting from (19), the following simple equation relating the ERR and the SIF based measures of mode mixity, phase angles ψ_G and ψ_K, can be deduced:

$$\cos(2\psi_G) = F(\varepsilon)\cos\left\{2(\psi_K + \psi_0(\Delta a/l, \varepsilon))\right\}. \tag{24}$$

The phase shift $\psi_0(\Delta a/l, \varepsilon)$ vanishes when $\Delta a/l = 2\exp[(\arctan(2\varepsilon) - \varphi(\varepsilon))/2\varepsilon]$ for an $\varepsilon \neq 0$, which gives the following interval for such values of Δa: $10.1169 < \Delta a/l < 10.8731$.

An in-depth study of new relations (19) and (24), recently presented by Mantič and París [82], showed that in a typical situation the following relation can be used as a first reasonable approximation: $\psi_G \approx \psi'_K$, $\psi'_K = |\psi_K + \psi_0(\Delta a/l, \varepsilon) + n\pi|$ with n being an integer number (usually $n = 0, \pm 1$) giving $0 \le \psi'_K \le \pi/2$. However, an important consequence of the fact that $F(\varepsilon) > 1$

for $\varepsilon \neq 0$ is that the oscillating values of $G_{\mathrm{I}}^{\mathrm{int}}(\Delta a)$ and $G_{\mathrm{II}}^{\mathrm{int}}(\Delta a)$ surprisingly achieve slightly negative values for some intervals of Δa as $\Delta a \to 0$. Notice that for such Δa the phase angle ψ_G cannot be represented, in view of (23), by a real number. These facts, which apparently have not previously been mentioned by other authors, might question the concept of 'energetic' mode mixity when applied to interface cracks. Therefore, a further study to establish physical reasons for these unexpected aspects of the open model of interface cracks will be required.

2.1.2 Contact model

In order to overcome inconsistencies of the open model, Comninou [19] developed an alternative model, usually referred to as the *contact model*, admitting the existence of one connected frictionless contact zone at each interface crack tip and one open part separating both contact zones. As a consequence of this hypothesis, instead of an infinite number of zones where interpenetrations occur in the open model at a crack tip, for $\beta \neq 0$, one connected near-tip contact zone appears. Solution of this model, whose uniqueness was proved by Shield [116], is the only totally physically acceptable solution of an interface crack problem under the assumptions adopted here: linear elastic behavior and an abrupt change along the interface (of zero thickness) between the perfectly bonded and debonded parts.

Due to the presence of a near-tip contact, no fracture Mode I SIF arises ahead of the crack tip, $K_{\mathrm{I}} = 0$. Thus, the interface crack grows in Mode II exclusively.

Stresses in the contact model are square root singular as at a crack tip placed in a homogenous material. However, when $\beta \neq 0$, the basic features of the near-tip stress states are very different from those known for the homogenous case: shear stresses ahead of the crack tip and compressions at the contact zone are singular, and both normal stresses (parallel and perpendicular to the interface) are bounded ahead of the crack tip. Furthermore, the near-tip singular elastic state is uniparametric, being governed by one multiplicative constant represented by the fracture Mode II SIF: K_{II}^{C}. Hence, for a particular bimaterial, relations between values of singular stresses are independent of the far-field load configuration.

With reference to the other extreme of the near-tip contact zone, Comninou and Dundurs [23] proved that the transition from this contact zone where crack faces slip to the zone where these crack faces are separated has to be smooth with vanishing contact pressure according to the square root law at the separation point.

According to Comninou [19] asymptotic series expansion, singular tractions acting on the interface at the right-hand crack tip as shown in fig. 2 are expressed as

$$\sigma_{xy}(r,0) = \sigma_{xy}^{\mathrm{sing}}(r,0) + O(\sqrt{r}) = \frac{K_{\mathrm{II}}^{C}}{\sqrt{2\pi r}} + O(\sqrt{r}), \quad \text{for } r \to 0, \tag{25}$$

$$\sigma_{yy}(r,\pm\pi) = \sigma_{yy}^{\mathrm{sing}}(r,\pm\pi) + O(1) = -\frac{\beta K_{\mathrm{II}}^{C}}{\sqrt{2\pi r}} + O(1) \leq 0, \quad \text{for } r \to 0. \tag{26}$$

An important consequence of the inequality in (26), implied by a requirement of near-tip compressive stresses between crack faces, is that

$$\beta K_{\mathrm{II}}^{C} \geq 0. \tag{27}$$

Therefore, the sign of K_{II}^{C} depends only on the bimaterial mismatch parameter β, being independent of the far-field load direction.

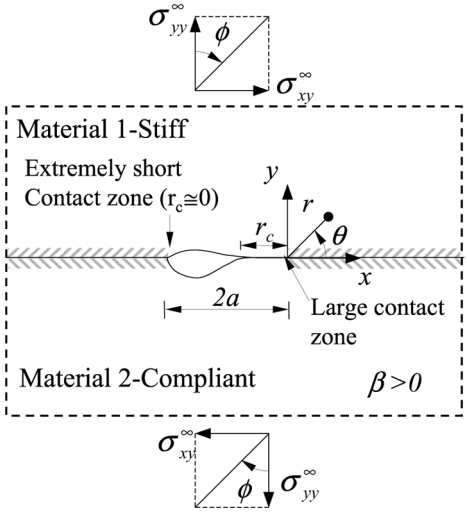

Figure 2: An interface crack subjected to a tension-shear load with a large and an extremely short contact zone.

Comninou [19] asymptotic expressions imply that the near-tip relative slip between the crack faces $\Delta u_x(r) = u_x(r, \theta = \pi) - u_x(r, \theta = -\pi)$ is expressed by:

$$\Delta u_x(r) = \Delta u_x^{\text{sing}}(r) + O(r) = \frac{8K_{\text{II}}^C}{\cosh^2(\pi\varepsilon)E^*}\sqrt{\frac{r}{2\pi}} + O(r), \quad \text{for } r \to 0, \tag{28}$$

hence the only allowed direction of the near-tip relative slip is defined by the relation $\beta \Delta u_x(r) \geq 0$ for $r \to 0$.

Starting from expressions(12)–(14) and (15), taking into account that here $G_{\text{I}}^{\text{int},C}(\Delta a) = 0$, applying (25), (28) and formula (18), with $\varepsilon = 0$, an Irwin-type expression for the total ERR due to an interface crack growth with frictionless contact at the crack tip is obtained:

$$G^{\text{int},C} = \lim_{\Delta a \to 0} G_{\text{II}}^{\text{int},C}(\Delta a) = \frac{(K_{\text{II}}^C)^2}{\cosh^2(\pi\varepsilon)E^*}. \tag{29}$$

The singular term in the asymptotic expansion of the near-tip stress field is expressed as:

$$\sigma_{ij}^{\text{sing}}(r, \theta) = \frac{K_{\text{II}}^C}{\sqrt{2\pi r}}\sigma_{ij}^C(\theta, \beta), \quad -\pi \leq \theta \leq \pi, \tag{30}$$

$$u_i^{\text{sing}}(r, \theta) = \frac{K_{\text{II}}^C}{2G_k}\sqrt{\frac{r}{2\pi}}u_i^C(\theta, \beta, \kappa_k), \quad \theta_k^- \leq \theta \leq \theta_k^+, \tag{31}$$

where $\theta_k^- = 0, -\pi$, and $\theta_k^+ = \pi, 0$ $(k = 1, 2)$. Universal dimensionless functions σ_{ij}^C and u_i^C were deduced by Comninou [19] in polar coordinates. When $\beta = 0$ this term reduces to the classical expression for a crack in a homogenous material subjected to fracture Mode II, independently of α value. Thus, $\sigma_{ij}^C(\theta, 0)$ in (30) equals both $\sigma_{ij}^{\text{II}}(\theta, 0)$ in (10) and $\sigma_{ij}^{\text{II}}(\theta)$ in (55).

From a typical angular variation of functions σ_{ij}^C shown in fig. 3 it can be observed that singular compressions $\sigma_{\theta\theta}^{\text{sing}}(r, \theta) < 0$ act in the stiffer material ($0 < \theta \leq \pi$ for $\beta > 0$ (fig. 2)) for all values

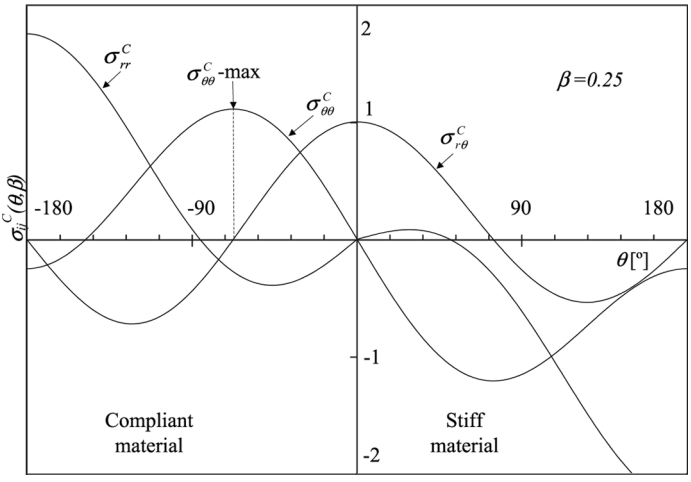

Figure 3: Angular variation of $\sigma^C_{\theta\theta}(\theta,\beta)$, $\sigma^C_{r\theta}(\theta,\beta)$ and $\sigma^C_{rr}(\theta,\beta)$ in the contact model for an isotropic bimaterial with $\beta = 0.25$.

of the polar angle θ. Therefore, it can be expected that a possible kink onset from an initially closed crack tip will be directed into the more compliant material ($-\pi \leq \theta < 0$ for $\beta > 0$). Additionally, fig. 3 reveals that the local maximum or minimum of the opening stress $\sigma^{\text{sing}}_{\theta\theta}(r,\theta)$ is achieved at values of the polar angle θ where the shear stress $\sigma^{\text{sing}}_{r\theta}(r,\theta)$ vanishes. This fact is a consequence of the following relation:

$$\frac{\partial \sigma^C_{\theta\theta}(\theta,\beta)}{\partial \theta} = -\frac{3}{2}\sigma^C_{r\theta}(\theta,\beta), \tag{32}$$

which follows from the expressions of the singular stresses presented by Comninou [19].

With reference to a priori unknown near-tip contact zone extent r_c, Hills and Barber [53] showed that the ratio between the r_c and the interpenetration zone size r_i can be approximated by a very weak function of ε:

$$r_c/r_i = 4e^{-\arctan(2\varepsilon)/\varepsilon} \tag{33}$$

in the case where both zones are sufficiently small in comparison with the characteristic length of problem geometry r_g, i.e. $r_c, r_i \ll r_g$. According to (33), ratio r_c/r_i varies between 0.541 for vanishing ε and 0.584 for $\varepsilon = 0.175$.

A striking consequence of relation (27) is that in the vicinity of the crack tip the local singular elastic solution has for a bimaterial system the same shape independently of the far-field loading. Therefore, the near-tip slip can be performed in one direction only, which depends on the sign of β, see an in-depth analysis by Comninou and Dundurs [23]. When the global imposed shear loading agrees with this intrinsically allowed slip direction a relatively large near-tip contact zone may take place. However, when the applied global load tends to originate slip opposite to the allowed near-tip slip direction, only a very small contact zone, typically of subatomic size, appears at this tip. The two cases of allowed and not allowed near-tip slip directions are illustrated in fig. 4.

A gap, sometimes referred to as a 'bubble', appears between two contact zones sliding in opposite directions, the microscopic one at the crack tip in the intrinsic direction and the macroscopic one in the direction imposed by the load. The slope of the relative normal displacements

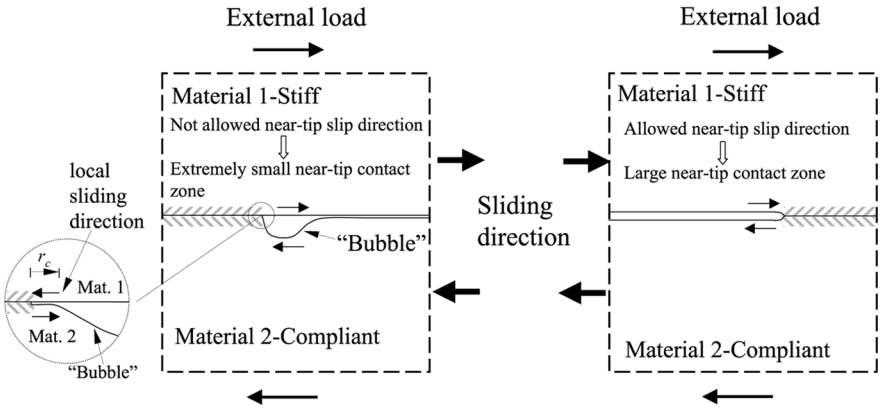

Figure 4: Intrinsically allowed and not allowed slip direction near a closed interface crack tip.

in the interface near the microscopic contact zone is very large. This behavior of an interface crack solution was first studied by Comninou [21], Comninou and Schmuesser [24], Gautesen and Dundurs [40] in interface cracks between two half-planes, and further discussed by Leguillon [70] and Audoly [6]. As a consequence, asymptotic singular solution of the contact model in presence of the 'bubble' extremely close to the crack tip becomes physically meaningless, such situations definitely fulfill SSC conditions, no near-tip contact zone is observable in experiments and, thus, the locally open model is adequate for analysis and predictions of crack behavior in such situations.

2.2 Orthotropic bimaterials

Plane interface crack problems in anisotropic, and in particular orthotropic, bimaterials were studied by many authors starting from the late sixties, see Deng [30] and Ting [132] for comprehensive review works.

Consider the following form of the three-dimensional stress-strain law for a linear elastic material written in the contracted Voigt notation: $\varepsilon_i = s_{ij}\sigma_j$ $(i,j = 1,\ldots,6)$, where s_{ij} are elastic compliances (see Ting [132]). Then, the plane stress-strain law for an orthotropic material in which the planes of material symmetry coincide with the coordinate planes is expressed as:

$$\begin{bmatrix} \varepsilon_{xx} \\ \varepsilon_{yy} \\ 2\varepsilon_{xy} \end{bmatrix} = \begin{bmatrix} s'_{11} & s'_{12} & 0 \\ s'_{12} & s'_{22} & 0 \\ 0 & 0 & s'_{66} \end{bmatrix} \begin{bmatrix} \sigma_{xx} \\ \sigma_{yy} \\ \sigma_{xy} \end{bmatrix}, \tag{34}$$

where

$$s'_{ij} = s_{ij} - \frac{s_{i3}s_{3j}}{s_{33}} \quad (i,j = 1,2,6) \tag{35}$$

represent reduced elastic compliances for plane strain deformations, and

$$s'_{ij} = s_{ij} \quad (i,j = 1,2,6) \tag{36}$$

for plane stress deformations.

Let material parameters $s_{\pm}$ be defined as follows:

$$s_{\pm} = \sqrt{\sqrt{s'_{11}s'_{22}} \pm \left(s'_{12} + s'_{66}/2\right)}. \tag{37}$$

From the positive definiteness of strain energy it follows that s_+ is always positive.

Let $\mathbf{L}$ and $\mathbf{S}$ denote the real valued Barnett-Lothe tensors [132] of the orthotropic material considered. Then, $\mathbf{L}^{-1}$ and $\mathbf{SL}^{-1}$ can be expressed as:

$$\mathbf{L}^{-1} = \sqrt{2}s_+ \begin{bmatrix} \sqrt{s'_{11}} & 0 \\ 0 & \sqrt{s'_{22}} \end{bmatrix}, \tag{38}$$

$$\mathbf{SL}^{-1} = \left(\sqrt{s'_{11}s'_{22}} + s'_{12}\right) \begin{bmatrix} 0 & -1 \\ 1 & 0 \end{bmatrix}. \tag{39}$$

Consider now a crack located at the interface between two dissimilar orthotropic materials, as in fig. 1, where $y > 0$ for material 1 and $y < 0$ for material 2. Magnitudes associated to each material will be denoted by a subindex giving the material number.

Let

$$\mathbf{D} = \begin{bmatrix} D_{11} & 0 \\ 0 & D_{22} \end{bmatrix} = \mathbf{L}_1^{-1} + \mathbf{L}_2^{-1} \quad \text{and} \quad \mathbf{W} = \begin{bmatrix} 0 & -w \\ w & 0 \end{bmatrix} = \mathbf{S}_1\mathbf{L}_1^{-1} - \mathbf{S}_2\mathbf{L}_2^{-1}. \tag{40}$$

Notice that $\mathbf{D}$ is a symmetric positive definite matrix and $\mathbf{W}$ is an antisymmetric matrix. The positive definite Hermitian matrix $\mathbf{D} - i\mathbf{W}$ associated to the bimaterial considered will be fundamental in characterizing elastic interface crack solutions (see Ting [132]). The dimensionless matrix

$$\mathbf{D}^{-1}\mathbf{W} = \begin{bmatrix} 0 & -\frac{w}{D_{11}} \\ \frac{w}{D_{22}} & 0 \end{bmatrix} \tag{41}$$

is called the *mismatch matrix* and the generalized Dundurs mismatch parameter β introduced by Ting [133] is defined as:

$$\beta = -\frac{w}{\sqrt{D_{11}D_{22}}}, \quad |\beta| < 1. \tag{42}$$

Notice that for an isotropic bimaterial, like that studied in Section 2.1.1:

$$\mathbf{D} = \frac{4}{E^*}\mathbf{I}, \quad \mathbf{W} = -\frac{4\beta}{E^*}\begin{bmatrix} 0 & -1 \\ 1 & 0 \end{bmatrix} \quad \text{and} \quad \mathbf{D}^{-1}\mathbf{W} = -\beta\begin{bmatrix} 0 & -1 \\ 1 & 0 \end{bmatrix}. \tag{43}$$

2.2.1 Open model

The following short explanation of the open model of interface cracks in orthotropic bimaterials is based on two substantial contributions due to Wu [146] and Suo [127]. In these works two different, although in fact equivalent, approaches to represent near-tip elastic fields were developed. The present explanation follows Wu's approach although some advantageous aspects of Suo's approach with reference to a measure of fracture mode mixity are applied.

A dimensionless matrix $\mathbf{R}[c]$ given as a function of a complex number c, introduced by Wu [146]:

$$\mathbf{R}[c] = \mathrm{Re}[c]\mathbf{I} + \beta^{-1}\mathrm{Im}[c]\mathbf{D}^{-1}\mathbf{W} = \begin{bmatrix} \mathrm{Re}[c] & \mathrm{Im}[c]\sqrt{\frac{D_{22}}{D_{11}}} \\ -\mathrm{Im}[c]\sqrt{\frac{D_{11}}{D_{22}}} & \mathrm{Re}[c] \end{bmatrix} \tag{44}$$

will be applied in the following expressions of the near-tip elastic solutions in the open model of an interface crack. It can be shown that $\mathbf{R}[1] = \mathbf{I}$ and $\mathbf{R}[c_1]\mathbf{R}[c_2] = \mathbf{R}[c_1 c_2]$. As follows from the explicit expression of the matrix in (44), $\mathbf{R}[c]$ is in fact independent of $\mathbf{W}$.

Introducing a characteristic length l, as in Section 2.1.1, the near-tip traction vector ahead of the crack tip along the interface can be expressed as (Wu [146]):

$$\begin{bmatrix}\sigma_{xy}\\ \sigma_{yy}\end{bmatrix}(r,0) = \begin{bmatrix}\sigma_{xy}^{\text{sing}}\\ \sigma_{yy}^{\text{sing}}\end{bmatrix}(r,0) + O(1)$$
$$= \frac{1}{\sqrt{2\pi r}}\mathbf{R}\left[\left(\frac{r}{l}\right)^{i\varepsilon}\right]\hat{\mathbf{K}} + O(1), \quad \text{for } r \to 0, \quad \hat{\mathbf{K}} = \begin{bmatrix}\hat{K}_2\\ \hat{K}_1\end{bmatrix}, \tag{45}$$

and the near-tip relative displacement across the crack as

$$\begin{bmatrix}\Delta u_x\\ \Delta u_y\end{bmatrix}(r) = \begin{bmatrix}\Delta u_x^{\text{sing}}\\ \Delta u_y^{\text{sing}}\end{bmatrix}(r) + O(r)$$
$$= \sqrt{\frac{r}{2\pi}}\frac{2\mathbf{D}}{\cosh(\pi\varepsilon)}\mathbf{R}\left[\frac{1}{1+2i\varepsilon}\left(\frac{r}{l}\right)^{i\varepsilon}\right]\hat{\mathbf{K}} + O(r), \quad \text{for } r \to 0, \tag{46}$$

where the oscillation index ε of the interface crack is given as in (4). Notice that in view of (42) there is no similar limit for ε to that valid for isotropic bimaterials (see Section 2.2.1.)

Explicit expressions of the singular oscillatory term in the expansion of the near-tip stress and displacement fields, analogous to (10–11), can be found for instance in Wu [148].

Although there are other definitions of the SIF used for interface cracks in orthotropic bimaterials (e.g. Suo [127]), the advantage of the present definition due to Wu [146] is that it reduces, as ε vanishes, to the classical SIF definition in homogenous orthotropic solids by Sih *et al*. [119]. For a revision of different definitions of the SIFs at interface cracks in anisotropic bimaterials see Hwu [57].

As follows from (45) the SIFs $\mathbf{K}'$ and $\mathbf{K}$ associated to two different reference lengths l' and l respectively are related by:

$$\hat{\mathbf{K}}' = \mathbf{R}\left[\left(\frac{l'}{l}\right)^{i\varepsilon}\right]\hat{\mathbf{K}}. \tag{47}$$

The phase angle of the SIF as a measure of the mode mixity (see Section 2.1.1) can be defined, in a standard way, by $\hat{\psi}_K = \arg(\hat{K}_1 + i\hat{K}_2)$ or equivalently in terms of stresses as $\tan\hat{\psi}_K = \sigma_{xy}^{\text{sing}}/\sigma_{yy}^{\text{sing}}(l,0)$. However, in order to maintain the phase shift rule (8) it is necessary to modify this definition using a scale factor, as discussed by Suo [127] and Wang *et al*. [143], in the following way: $\psi_K = \arg(\hat{K}_1 + i\sqrt{D_{11}/D_{22}}\hat{K}_2)$ or in terms of stresses as $\tan\psi_K = \sqrt{D_{11}/D_{22}}\sigma_{xy}^{\text{sing}}/\sigma_{yy}^{\text{sing}}(l,0)$. The disadvantage of the last definition is that it does not reduce to the phase angle of the classical SIF in homogenous orthotropic solids for vanishing ε when $D_{11} \neq D_{22}$. A simple relation existing between these two phase angles, $\tan\psi_K = \sqrt{D_{11}/D_{22}}\tan\hat{\psi}_K$, may be used where required.

By substituting (45)–(46) into (13)–(14) the total ERR G^{int} in (12) is expressed as (Hwu [57] and Wu [146]):

$$G^{\text{int}} = \frac{1}{4\cosh^2(\pi\varepsilon)}\hat{\mathbf{K}}^T\mathbf{D}\hat{\mathbf{K}} = \frac{D_{22}\hat{K}_1^2 + D_{11}\hat{K}_2^2}{4\cosh^2(\pi\varepsilon)}, \tag{48}$$

which reduces to (16) for an isotropic bimaterial. It is easy to show that whereas G^{int} is independent of the choice of the characteristic length l [146], the module of $\hat{\mathbf{K}}$ varies with l.

2.2.2 Contact model

Comninou frictionless contact model (originally developed for isotropic bimaterials (see Section 2.1.2)) has been generalized to anisotropic, or in particular orthotropic, materials in the works of Wu [147, 149], Deng [27, 28, 30], Lee and Gao [68], and Ting [132] among others.

Relations for singular tractions acting along the interface at the right-hand crack tip, as shown in fig. 2, coincide with those given in (25)–(26) together with the inequality in (27) when β is taken from (42).

The near-tip relative slip between the crack faces is expressed analogously to (28) as:

$$\Delta u_x(r) = \Delta u_x^{\text{sing}}(r) + O(r) = \frac{2D_{11}K_{\text{II}}^C}{\cosh^2(\pi\varepsilon)}\sqrt{\frac{r}{2\pi}} + O(r), \quad \text{for } r \to 0. \tag{49}$$

The Irwin-type expression of the total ERR due to an interface crack extension, analogous to that in (29), takes the form:

$$G^{\text{int},C} = \lim_{\Delta a \to 0} G_{\text{II}}^{\text{int},C}(\Delta a) = \frac{D_{11}(K_{\text{II}}^C)^2}{4\cosh^2(\pi\varepsilon)}. \tag{50}$$

It should be mentioned that Wu [147] proved the existence of a correspondence between solutions of the contact model for an interface crack in an orthotropic and an isotropic bimaterial. Through this correspondence, the SIF and the sizes of the contact zones associated to an interface crack in an orthotropic bimaterial can be obtained from these quantities for an equivalent interface crack problem in an isotropic bimaterial.

2.3 Remarks on application of the interface crack models

The current understanding of the problem of interface cracks is that both, open and contact, linear-elastic models are important in analysis and prediction of interface crack propagation. None of these models is free of some inconsistencies and/or difficulties in its application to modeling behavior of interface cracks. There are situations where application of only one of the above linear elastic models is adequate. However, there are also intermediate situations where both models may be applied providing similar results.

Although, the solution of the contact model, as opposed to the open model solution, is the only physically correct solution (within the context of linear elasticity) of the interface crack problem regardless of the geometry and the loading conditions, this model is not always adequate to characterize fracture. From an operative point of view for instance, the previous statement would correspond to the fact that the open solution is linear with load, thus being relatively easily obtained by FEM or BEM, whereas the frictionless contact solution is only a homogeneous function of load, requiring application of a non-linear algorithm to evaluate the a priori unknown contact zone length. However, as will be explained in the following, the adequacy of the contact model to characterize an interface crack growth basically depends on the relation between the near-tip contact zone extent r_c and the size of the zone of nonlinear material response (including, e.g., fracture process zone) r_p (Rice [112], Hills and Barber [53]).

As explained above, SSC conditions refer to a situation where r_c is smaller than r_p. Then, the near-tip singular solution of the open model contains all the relevant information. In particular, the singular term of the open model solution, governed by the complex SIF $\hat{K}$, is suitable for representing a fracture mode mixity at the crack tip under SSC conditions, in opposition to the singular term of the contact solution, which is governed by only one parameter, SIF K_{II}^C, and thus

it is not able to represent any fracture mode mixity. Note that under SSC conditions $|K| \cong K_{\mathrm{II}}^{C}$ and equivalently $G^{\mathrm{int}} \cong G^{\mathrm{int},C}$.

The above described disadvantage of the contact model is also reflected in the discontinuity of the singular term when $\beta \to 0$. Singular term of the near-tip contact solution governed by one SIF for $\beta \neq 0$, changes in the limit to the singular term governed by two classical SIFs for $\beta = 0$. This implies, for instance, that when $K_{\mathrm{I}} = 1$ and $K_{\mathrm{II}} = 0$ for $\beta = 0$, then introducing the most insignificant material discontinuity yields $K_{\mathrm{I}}^{C} = 0$ and $K_{\mathrm{II}}^{C} \approx 1$ for $\beta \neq 0$ (Hills *et al*. [54]). This strange behavior is associated to the extremely small (subatomic) size of the near-tip contact zones (and of zones dominated by K_{II}^{C} as well) for $\beta \approx 0$ which implies that other asymptotically non-singular terms start to contribute significantly to the solution value at small physically relevant distances from the crack tip.

On the other hand, when r_c is significantly larger than r_p, the open model solution and the contact solution differ significantly outside the zone of nonlinear material response, and it appears that only the contact solution is able to provide useful information relevant to micromechanics of fracture Mode II present at the crack tip. Thus, in such situations the contact model is adequate to analyze and predict interface crack growth.

Therefore, in a general practical numerical procedure for interface crack analysis both models should be included, in a way similar to that proposed by Hills and Barber [53] and Hills *et al*. [54] and implemented by Liu and Feng-Chen [74]. In such a procedure, both models are competing between each other, the open model being applied where SSC conditions hold ($r_i \ll r_p$ and consequently also $r_c \ll r_p$), otherwise the contact model is applied.

In fact, in presence of a significant shear load in case of burried interface cracks, SSC conditions are typically fulfilled only at one crack tip, where an extremely short contact zone is present, while at the other tip a large contact zone of length comparable to the total crack length appears (e.g. tests with Brazilian nut sandwich specimen by Banks-Sills and Ashkenazi [8] and Yuuki *et al*. [151], among others). Thus, when analyzing this type of problem, one model is suitable at one crack tip and the other at the opposite crack tip. Another situation, where both models are applied, appears sometimes during modeling of an interface crack growth, a switch between models being required. The numerical procedure may start, for instance, with the open model as the adequate one and when the crack extends further the contact model may become more suitable, e.g. due to a change of the load orientation with respect to the crack tip following a curved interface (see Section 7).

3 Interface crack propagation and kinking

The possibility of predicting accurately whether a bi-material interface crack will propagate along the interface, kink out of the interface, or not propagate at all, will be discussed in this section. As in the rest of the paper, the considerations are restricted to plane situations. Additionally, the results presented in this section are restricted to isotropic materials. This in spite of the fact that in Section 6a case of an interface crack in an orthotropic bi-material is studied, but the objective of that study does not involve kinking. In fact, the authors are only aware of a few works dealing with application of criteria for interface crack propagation and kinking in anisotropic bi-materials: Miller and Stock [88], Wang [142] and Wang *et al*. [143].

The effect of the finite stress parallel to the interface (so-called T-stress) in kinking of an interface crack will not be considered in the following analytical review of the available theory. Thus, the applicability of the results of this study would be in relation to the initiation of the kinked crack. In Section 7 the representability of the singular term and the influence of T-stress

in the energy released by a kinked crack are evaluated in the case studied. An influence of the T-stress on the interface crack propagation was studied by He *et al*. [5] in isotropic bimaterials and by Wang [142] in anisotropic bimaterials.

3.1 Crack paths in homogeneous isotropic materials

Although as follows from a large number of recent studies and experiments (Miller and McDowell [87], Pook [109]), two fundamentally distinct classes of crack growth, maximum principal stress dominated (crack growth in Mode I) and shear-dominated (crack growth in Mode II), are under consideration at the time, the present section is concerned with common Mode I crack growth, which assumes traction-free crack lips in the vicinity of the crack tip. Additionally, static load and SSY conditions are assumed. Several well-known criteria for crack growth prediction in homogeneous isotropic solids in such a situation, which relate the local stress field at the crack tip to the crack extension, will be briefly presented and discussed, for both smooth and kinked crack paths.

3.1.1 Crack growth following a smooth path

The path of a smooth propagation of a crack, under a certain state of load which originates a near-tip stress field governed in general by SIFs K_{I} and K_{II}, has been proposed to obey the three proved equivalent propagation criteria: *maximum energy release rate criterion* (MERR) by Erdogan and Sih [35], *local symmetry criterion* (LS) ($K_{\mathrm{II}} = 0$) by Goldstein and Salganik [46] and *maximum* K_{I} *criterion* ($\mathrm{MK_I}$), e.g., Broberg [16]. In simple terms it means that crack propagates maximizing the energy release rate in pure opening Mode I. Following this path the fracture criterion for initiation of crack advance takes the classical form:

$$K_{\mathrm{I}} = K_{\mathrm{I}c}, \quad G_{\mathrm{I}} = G_{\mathrm{I}c}, \tag{51}$$

where $G_{\mathrm{I}c} = K_{\mathrm{I}c}^2/E'$ represents the fracture toughness of the material in Mode I.

Note that Amestoy and Leblond [2], considering a smoothly propagating crack under proportional loading, deduced, applying LS criterion, a general equation for smooth crack path, which predicts path curvature at any regular point.

3.1.2 Crack kinking

Consider a stationary crack subjected to a mixed mode loading ($K_{\mathrm{II}} \neq 0$) with a local mode mixity defined by angle ψ_K, $\tan\psi_K = K_{\mathrm{II}}/K_{\mathrm{I}}$. Such a crack may kink, changing abruptly its direction of propagation. A straight kink crack of a small length b with SIFs $k_m(\theta, b)$ ($m = \mathrm{I}, \mathrm{II}$) associated to its tip, as shown in fig. 5, is considered in the present work. There are several proposals to predict kink angle θ_{kink}, the following four being those most commonly used: MERR, LS and $\mathrm{MK_I}$ criteria, which are only approximately equivalent in this case (see Melin [84], He and Hutchinson [50], Amestoy and Leblond [2], Broberg [17]), and the *maximum circumferential stress criterion* (MCS) by Erdogan and Sih [35].

MERR, LS and $\mathrm{MK_I}$ criteria require to evaluate SIFs $k_m(\theta)$ to be evaluated at an infinitesimal kinked extension. They are obtained evaluating limits of $k_m(\theta, b)$ for a vanishing kink length b:

$$k_m(\theta) = \lim_{b\to 0} k_m(\theta, b), \quad m = \mathrm{I}, \mathrm{II}, \tag{52}$$

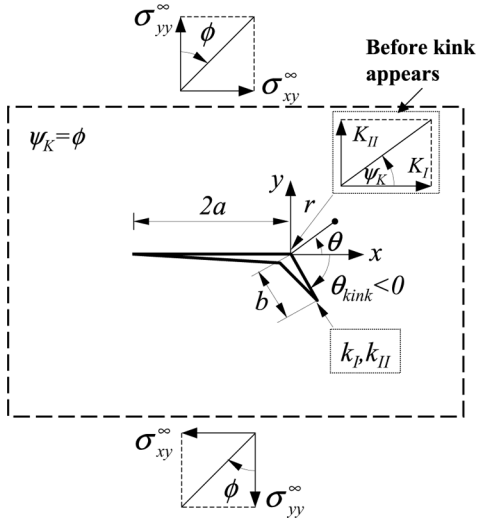

Figure 5: Crack kinking in a homogeneous material due to a mixed mode loading.

as linear combinations of the SIFs of the parent crack K_{I} and K_{II}:

$$k_{\mathrm{I}}(\theta) = C^h_{11}(\theta)K_{\mathrm{I}} + C^h_{12}(\theta)K_{\mathrm{II}},$$
$$k_{\mathrm{II}}(\theta) = C^h_{21}(\theta)K_{\mathrm{I}} + C^h_{22}(\theta)K_{\mathrm{II}}, \tag{53}$$

where superindex h means homogeneous material. Dimensionless coefficients $C^h_{ij}(\theta)$ were computed in tabulated form by Amestoy *et al.* [1], Hayashi and Nemat-Nasser [49] and Melin [86], and series expansions of these coefficients were deduced through extensive analytic calculations by Amestoy and Leblond [2]. These coefficients are universal in the sense that they apply to arbitrary geometry of the body and crack, material and loading.

In contrast with the above cumbersome procedure, application of MCS criterion is very simple, only knowledge of the analytic expression of the asymptotic singular term of the stress field at the parent crack tip before the kink onset, $\sigma^{\mathrm{sing}}_{ij}(r,\theta)$, being required.

In order to write explicit forms of the former criteria, let the energy release rate at an infinitesimal kinked extension be expressed as

$$G^{\mathrm{kink}}(\theta) = \left(k^2_{\mathrm{I}}(\theta) + k^2_{\mathrm{II}}(\theta)\right)/E', \tag{54}$$

and the asymptotic singular stress field at the original crack tip (equivalent to (10) for $\varepsilon = 0$ there) as

$$\sigma^{\mathrm{sing}}_{ij}(r,\theta) = \frac{1}{\sqrt{2\pi r}}\left(K_{\mathrm{I}}\sigma^{I}_{ij}(\theta) + K_{\mathrm{II}}\sigma^{\mathrm{II}}_{ij}(\theta)\right). \tag{55}$$

Then, the above criteria can be simply expressed respectively as:

$$\text{(MERR)} \qquad \left.\frac{\partial \mathrm{G}^{\mathrm{kink}}}{\partial\theta}\right|_{\theta=\theta_{\mathrm{kink}}} = 0 \quad \text{and} \quad \left.\frac{\partial^2 \mathrm{G}^{\mathrm{kink}}}{\partial^2\theta}\right|_{\theta=\theta_{\mathrm{kink}}} < 0, \tag{56}$$

$$\text{(LS)} \qquad k_{\mathrm{II}}(\theta_{\mathrm{kink}}) = 0, \tag{57}$$

$$\text{(MK}_{\mathrm{I}}\text{)} \qquad \left.\frac{\partial k_{\mathrm{I}}}{\partial \theta}\right|_{\theta=\theta_{\mathrm{kink}}} = 0 \quad \text{and} \quad \left.\frac{\partial^2 k_{\mathrm{I}}}{\partial^2 \theta}\right|_{\theta=\theta_{\mathrm{kink}}} < 0, \tag{58}$$

$$\text{(MCS)} \qquad \left.\frac{\partial \sigma_{\theta\theta}^{\mathrm{sing}}}{\partial \theta}\right|_{\theta=\theta_{\mathrm{kink}}} = 0 \quad \text{and} \quad \left.\frac{\partial^2 \sigma_{\theta\theta}^{\mathrm{sing}}}{\partial^2 \theta}\right|_{\theta=\theta_{\mathrm{kink}}} < 0. \tag{59}$$

All these criteria yield fairly similar results. Thus, for instance, for a straight crack subjected to a pure Mode II, $K_{\mathrm{I}} = 0$ and for example $K_{\mathrm{II}} > 0$, the kink angles predicted by these criteria respectively are: $\theta_{\mathrm{kink}} = -75.8°, -77.3°, -76.6°$ and $-70.5°$. Consequently experimental results have not as yet provided a decisive argument in favour of any one of them (see e.g., Erdogan and Sih [35], Broberg [16], Vaughan [139]).

Supposing a kink direction obtained by one of the above criteria, the criterion for onset of crack growth is given by:

$$G^{\mathrm{kink}}(\theta_{\mathrm{kink}}) = G_c, \tag{60}$$

where G_c stands for the fracture toughness of the material. This criterion corresponds to classical crack propagation criterion written as

$$k_{\mathrm{I}}(\theta_{\mathrm{kink}}) = K_{\mathrm{I}c}, \tag{61}$$

if LS criterion has been previously applied to predict θ_{kink}.

As will be shown in the following, fracture criteria discussed above, although developed primarily for cracks in homogeneous materials, can be readily extended to interface cracks.

3.2 Interface crack paths

The problem of the growth of an interface crack subjected to a load is studied. This crack may grow by its further extension along the interface or kink out of the interface. Depending on the asymmetry of the material properties, interface cracks have a strong tendency to kink into one of the materials adjacent to the interface.

One complexity of interfacial fracture mechanics is that toughness of each constituent material and the interface itself, together with possibly substantially different fracture mechanisms of both materials and the interface itself (e.g. bonding a ductile and a brittle material) have to be taken into account.

It is believed that cracking path is defined by the local singular stress state at the parent crack tip and by the relation between fracture toughness of interface $G_{\mathrm{c}}^{\mathrm{int}}$ and fracture toughness of the material towards which the kink is directed $G_{\mathrm{c}}^{\mathrm{kink}}$. The competition between interface crack extension and kinking (assuming Mode I propagation after kink) can be formulated on the energetic basis comparing ratios of the corresponding energy release rates associated to a load level, G^{int} and G^{kink}, and the fracture toughness for extension and kinking (He and Hutchinson, [50]):

$$\frac{G^{\mathrm{int}}}{G_c^{\mathrm{int}}} > \frac{G^{\mathrm{kink}}}{G_c^{\mathrm{kink}}} \quad \Rightarrow \quad \text{extension}, \qquad \frac{G^{\mathrm{int}}}{G_c^{\mathrm{int}}} < \frac{G^{\mathrm{kink}}}{G_c^{\mathrm{kink}}} \quad \Rightarrow \quad \text{kink}. \tag{62}$$

Note that G^{kink} corresponds to a kink angle θ_{kink} predicted by a fracture criterion. Additionally, whereas G_c^{kink} is independent of θ_{kink} in isotropic materials, it may be a function of this angle in anisotropic materials.

As has been explained in Section 2, depending on the problem configuration, and in particular on the load direction, the contact zone size at an interface crack tip can be either relatively small with respect to the crack length (even extremely small of subatomic size), or it can have a finite and physically relevant length. Crack tips with a small contact zone can be effectively treated using the open crack model supposing SSC conditions while the contact model is required for those with a finite contact zone. Application of fracture criteria in these two models will be treated separately in the following sections.

3.2.1 Interface crack propagation under SSC conditions

Rice [112] and He and Hutchinson [50] proposed that under SSC conditions a prediction of the interface crack growth, extension or kinking, can be based on the singular crack tip field of the open model. Recall that the asymptotic crack tip field is defined by two parameters: either the real and imaginary part of the complex SIF $\hat{K} = \hat{K}_1 + i\hat{K}_2$ or, equivalently, by energy release rate G^{int} and the fracture mode mixity $\psi_K = \arg \hat{K}$. Recall that ψ_K depends on the choice of the reference length l. However, this dependence is relatively weak in the range of physically relevant scales for typical values of the oscillatory index ε (see (8)).

3.2.1.1 Interface crack extension When G_c^{int} is relatively small, the first inequality in crack path selection criterion (62) implies that the interface crack may be trapped at the interface and propagates along it in mixed fracture mode ($\psi_K \neq 0$). In such situations, G_c^{int} as a function of ψ_K can be measured. Strong dependence on the mode mixity of interface toughness $G_c^{\text{int}}(\psi_K)$ has been observed in extensive experiments performed starting from the late 1980s (e.g., Wang and Suo [144], Hutchinson and Suo [56], Liechti and Chai [73], Wang [141], Banks-Sills and Ashkenazi [8]). Interface toughness (equal to the total energy required to produce crack growth along the bonded line) depends on the mechanism of failure of the bimaterial system (the constituent materials, the possible interphase and the corresponding interfaces) and can be considered as a sum of the work of separation and the dissipation energy. It has been proposed (Evans *et al*. [36], Volinsky *et al*. [140]), that the separation work is independent of ψ_K whereas the dissipation energy is strongly dependent on ψ_K. Values of $G_c^{\text{int}}(\psi_K, l)$ (for simplicity usually written only as $G_c^{\text{int}}(\psi_K)$) for high values of ψ_K can be one order higher than those for near zero values of ψ_K.

It is clear from all the above considerations that ψ_K is an important parameter governing interface crack growth. Thus, rather than a single toughness value used to quantify fracture resistance of a homogeneous material (assuming that in a homogeneous material the crack will grow under Mode I), toughness values at a range of mode mixities characterize fracture resistance of an interface. This is a distinctive feature of interfacial fracture mechanics under SSC conditions in comparison with fracture mechanics of brittle homogeneous solids. A determined interface crack may have different mixities due to different loadings and even under a particular system of loads the mixity will change (in accordance with Section 2.1.2), with the growth of the crack.

Mechanisms contributing to dissipation energy depend on constituent materials and also on the way in which these materials are adhered (Evans *et al*. [36], Swadener *et al*. [129]). The most significant contribution is usually due to a plastic zone (Shih and Asaro [117], Tvergaard [135]), which will generally surround the fracture process governing separation if at least one constituent is a metal or polymer. Another form of dissipation energy at an interface crack is, for instance, asperity contact between crack faces. When thinking of an interface fracture criterion two options arise, to give G_c^{int} as a function of ψ_K or to define a failure locus in $(\hat{K}_1, \hat{K}_2)$-space. Several phenomenological laws for $G_c^{\text{int}}(\psi_K, l)$ were suggested in the past, the following expressions representing

two families of realistic ones (Hutchinson and Suo [56], Charalambides *et al*. [25]):

$$G_c^{\text{int}}(\psi_K, l) = G_1 \left(1 + (1-\lambda)\tan^2(\psi_K - \psi_0)\right), \tag{63}$$

$$G_c^{\text{int}}(\psi_K, l) = G_1 \left(1 + \tan^2(1-\lambda)(\psi_K - \psi_0)\right), \tag{64}$$

where G_1 is the fracture Mode I toughness (associated to the minimum value of $G_c^{\text{int}}(\psi_K, l)$), λ is an adjustable material parameter that reflects both plasticity in the crack tip as well as interface roughness ($\lambda = 1$ corresponds to an ideally brittle interface with no mixed-mode effect whereas a strong mode dependence exists when λ is small), and ψ_0 represents a phase shift. This shift may be modified by a different choice of the reference length l. In particular, defining a new reference length as $l' = le^{-\psi_0/\varepsilon}$ eliminates this shift. Typical forms of curves $G_{\text{c}}^{\text{int}}(\psi_K, l)$ and $G_{\text{c}}^{\text{int}}(\psi_K, l')$ are shown in fig. 6. This corresponds particularly to (63) with $\lambda = 0$. Note that experimental curves $G_{\text{c}}^{\text{int}}(\psi_K)$ do not need to be symmetric with respect to any vertical line due to the strong differences in the deformed configuration in the surrounding area of the predicted near-tip contact zones associated to different signs of ψ_K, as was explained in Section 2.1.2, and to the related asymmetry in the plastic dissipation, e.g. the volume of the near-tip plastic zone is different for different signs of ψ_K, see Liechti and Chai [73], Tvergaard and Hutchinson [136], Swadener and Liechti [128]. For interfaces, like glass/epoxy, (63) with $\lambda = 0$ represents a very good approximation of experimental results (see Liechti-Chai [73], Charalambides *et al*. [25], Banks-Sills and Ashkenazi [8]).

It is useful to observe that the particular graph of $G_c^{\text{int}}(\psi_K)$ shown in fig. 6 corresponds to a failure locus, given in this particular case by a straight line, in $(\hat{K}_1, \hat{K}_2)$-space (fig. 7). Although the $G_{\text{c}}^{\text{int}}(\psi_K)$ graph is that commonly used, linear regression might be applied to estimate G_1 and ψ_0 using the failure locus in the $(\hat{K}_1, \hat{K}_2)$-space. Note that this failure locus is rotated when another reference length l' is chosen.

Once $G_c^{\text{int}}(\psi_K, l)$ is determined experimentally, the criterion for onset of an interface crack extension along the interface can be written as

$$G^{\text{int}} = G_c^{\text{int}}(\psi_K, l), \tag{65}$$

where G^{int} is given by (15).

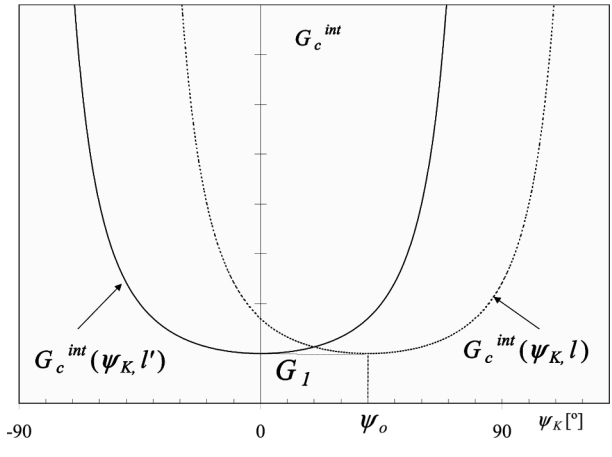

Figure 6: Interface toughness function.

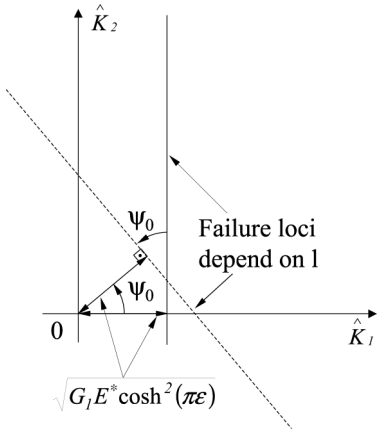

Figure 7: Graph of $\hat{K}_1$ versus $\hat{K}_2$ at interface fracture (Corresponds to eqn (63) for $\lambda = 0$).

As a summary, the fact that an interface crack may stay trapped at the interface, as a weak plane, in a mixed mode is the origin of the difficulties of Interfacial Fracture Mechanics. In a homogeneous material the "weak plane" is locally that associated to Mode I. Thus, while in homogeneous materials one number K_{Ic} is sufficient to characterize fracture toughness of one material under any load, here a functional dependence $G_c^{\text{int}}(\psi_K)$ is necessary to fully characterize the toughness of an interface. Toughness function $G_c^{\text{int}}(\psi_K)$ is a property of the interface and is independent of the specimen geometry and loading. This fact associated to mode mixity inherent to an interface crack substantially complicates the Interfacial Fracture Mechanics from an engineering point of view, perhaps even more than the oscillatory behavior of the linear elastic field.

3.2.1.2 Interface crack kinking Consider, as in Section 3.1.2, a straight kink crack of length b, small compared to the parent interface crack length $2a$ (fig. 8). We can assume that the kink crack onset and its angle θ_{kink} are determined by the near-tip stress field of the interface crack and by G_c^{kink}.

The difficulty with extension of the classical criteria for fracture in homogeneous solids discussed in Section 3.1.2 to the present case when $\beta \neq 0$ is associated to the oscillatory character of the singular elastic solution for the parent interface crack. As a consequence of this oscillatory character, these criteria do not predict a unique value of kink angle without specifying either a fixed kink crack length (criteria MERR, LS, MK_I) or the distance to the tip (criterion MCS) for which the criteria are evaluated (He and Hutchinson [50], Geubelle and Knauss [43, 44] and Makai *et al*. [89]). Different kink lengths or different distances to the tip will imply different kink angle values predicted by these criteria. Thus, an additional characteristic length scale is necessary to make predictions by these criteria unique. This characteristic length could be considered as a property of the bi-material and determined experimentally by computing the horizontal shift of the "master curve" to fit experimental data (θ_{kink}, ψ_K), Geubelle and Knauss [43].

He and Hutchinson [50] suggested, as a pragmatic way of overcoming the difficulties caused by the oscillatory character of the analytic solutions, downplaying the role of β by arbitrarily taking $\beta = 0$, when these solutions are applied to make predictions or interpret experiments, especially when β is small. They showed that such an approach is reasonable because the fracture variables of interest depend weakly on β.

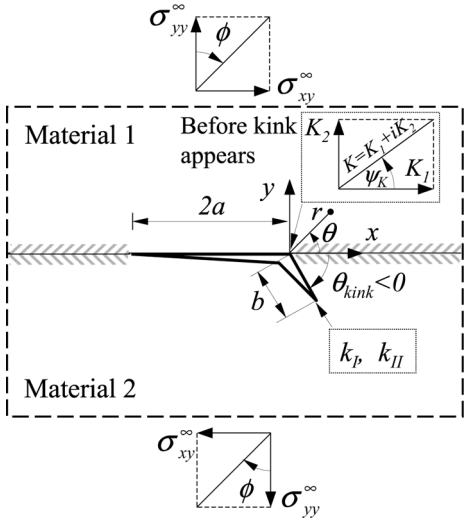

Figure 8: Interface crack kinking due to a mixed mode loading.

Once θ_{kink} is predicted by a certain criterion, (62) may be applied to the competition between kinking and further interface crack extension. For a discussion of competition between extension along interface and kinking see Yuuki *et al*. [151]. When, following a criterion, the predicted θ_{kink} is oriented into a sufficiently tough material, then as follows from (62) the interface crack will not kink, being trapped at the interface and will propagate in a mixed mode. There are, however, situations where interface crack kinking is not governed by (62), see an example given by Wang and Suo [144] and their explanations.

Let us now revise an application of the different criteria for predicting θ_{kink}. Recall that MCS criterion represents a very simple and operative option for θ_{kink} prediction, requiring only knowledge of the near-tip field of the parent crack, while MERR, LS or MK_I criteria require much more involved analytic and/or numerical calculations including kink crack modeling.

Geubelle and Knauss [43] analyzed prediction of θ_{kink} by MCS criterion. By substituting (10) into (59) θ_{kink} is given by the following implicit relation:

$$\tan\left(\psi_K + \varepsilon \ln \frac{r}{l}\right) = -\left[\frac{\mathrm{d}\sigma^{\mathrm{I}}_{\theta\theta}}{\mathrm{d}\theta}(\theta,\varepsilon) \Big/ \frac{\mathrm{d}\sigma^{\mathrm{II}}_{\theta\theta}}{\mathrm{d}\theta}(\theta,\varepsilon)\right]_{\theta=\theta_{\text{kink}}}. \tag{66}$$

Hence, the value of θ_{kink} varies with varying radius r of the circumference where $\sigma_{\theta\theta}$ is maximized. This radial dependence of θ_{kink} appears as a shift $\varepsilon \ln \frac{r}{l}$ of the "master curve" in the diagram of θ_{kink} versus ψ_K.

MERR, LS and MK_I criteria require an evaluation of SIFs at a kink crack. Applying a dimensional analysis, He and Hutchinson [50] deduced the expressions for SIFs at an infinitesimal kink crack as functions of the complex interfacial SIF $\widehat{K}$:

$$\begin{aligned} k_{\text{I}}(\theta,b) &= C^o_{11}(\theta,\alpha,\beta)\text{Re}[\hat{K}(b/l)^{i\varepsilon}] + C^o_{12}(\theta,\alpha,\beta)\text{Im}[\hat{K}(b/l)^{i\varepsilon}], \\ k_{\text{II}}(\theta,b) &= C^o_{21}(\theta,\alpha,\beta)\text{Re}[\hat{K}(b/l)^{i\varepsilon}] + C^o_{22}(\theta,\alpha,\beta)\text{Im}[\hat{K}(b/l)^{i\varepsilon}], \end{aligned} \tag{67}$$

which are equivalent to (53) for $\varepsilon \to 0$. According to (67) SIFs are oscillating with kink length b, and consequently no limit exists for $b \to 0$ when $\beta \neq 0$. He and Hutchinson [50] tabulated

coefficients C_{ij}^{o} in (67) for several pairs of α and β. They suggested maximum energy release rate criterion and considering, instead of the oscillating value of

$$G^{\text{kink}}(\theta, b) = \frac{k_{\text{I}}^2(\theta, b) + k_{\text{II}}^2(\theta, b)}{E'_{\text{kink}}}, \tag{68}$$

where E'_{kink} is the elasticity modulus for the material towards which the kink is directed, the following non b-dependent representative value

$$G^{\text{kink},*}(\theta) = G^{\text{kink}}(\theta, l), \tag{69}$$

where l is the above discussed characteristic length scale. Value of $G^{\text{kink},*}(\theta)$ associated to l, placed somewhere between maximum and minimum of $G^{\text{kink}}(\theta, b)$, gives a good approximation for several representative bi-materials with $\varepsilon \approx 0$.

He and Hutchinson [50] observed a strong influence of α and only a relatively weak influence of β on $G^{\text{kink},*}$ as a function of θ. Thus, considering MERR criterion, the effect of β on curves of θ_{kink} values, which are associated to the maximum value of $G^{\text{kink},*}$, versus ψ_K appears to be relatively weak as well.

He and Hutchinson [50] and Mukai *et al*. [89], observed that the more compliant the material into which the crack kinks, the larger the energy release rate. Conversely, if the crack kinks into relatively stiffer material the energy release rate is reduced.

Note that the relation between θ_{kink} and mode mixity ψ_K predicted by MERR criterion is not one-to one, because for a certain range of ψ_K the criterion predicts that maximum $G^{\text{kink},*}$ is achieved at the interface. Geubelle and Knauss [43] observed such a range of ψ_K when interface toughness G_c^{int} was comparable to at least the toughness of the weaker constituent. If G_c^{int} is much smaller than the toughness of either constituent, the crack will be trapped at the interface for even a wider range of ψ_K than before.

He and Hutchinson [50] compared also LS and MERR criteria, very similar predictions of θ_{kink} having typically been obtained, although there are situations where MERR criterion predicts extension along the interface while LS criterion would predict a kink at a high angle near a local maximum of $G^{\text{kink},*}$. Geubelle and Knauss [43] observed that differences between MCS and MERR criteria are higher than in homogeneous materials and that MERR criterion was more in accord with their experiments.

Finally, let us recall that while, according to (67), θ_{kink} predicted by MERR or LS criterion is a function of both mismatch parameters, α and β, this angle predicted by MCS criterion is only a function of β parameter.

3.2.2 Interface crack propagation from an initially closed crack tip

When SSC conditions are not fulfilled due to a physically relevant size of the contact zone at an interface crack tip, it is believed that a prediction of the interface crack growth, extension or kinking, can be based on the singular near-tip elastic solution of the contact model. A distinctive feature of the singular asymptotic term in contact model, in comparison with that in the open model, is that it is governed by one parameter only: real SIF K_{II}^{C}. Thus, the form of distribution of these singular stresses is always the same for a particular bi-material independently of the global problem configuration (geometry, loads, etc.), the magnitude of the stresses being given by a multiplicative constant represented by K_{II}^{C}.

In the present work only the frictionless contact model will be considered. For an analysis of a friction contact model of interface cracks, see Comninou [20], Comninou and Dundurs

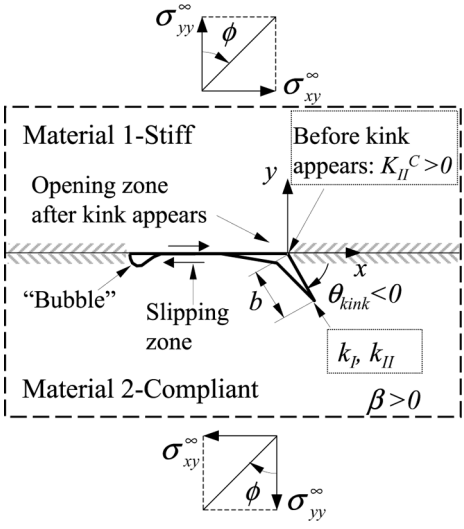

Figure 9: Interface crack kinking from an initially closed crack tip.

[23], Stringfellow and Freund [121], Deng [28, 29, 30], París *et al*. [101], Sun and Qian [126], Leguillon [70], Audoly [6] and Leblond and Frelat [67].

The fact that the local stress field depends only on one-parameter, has an important consequence for application of the above propagation criteria to kink angle θ_{kink} prediction. As in Section 3.2.1.2, a straight kink crack of length b small compared to the parent interface crack length $2a$, is considered here again (fig. 9). θ_{kink} predicted by a criterion will be independent of the global load configuration, assuming a sufficiently large contact zone is developed at the crack tip. Thus, for a particular bi-material, each criterion will predict only one value of θ_{kink}. Recall that this is the opposite to the situation when SSC conditions are fulfilled as was discussed in Section 3.2.1.2.

3.2.2.1 Interface crack extension In presence of a physically relevant near-tip contact zone ($r_c \gg r_p$), the mixity of the singular near-tip solution disappears and the fracture toughness does not require to be defined by a function of the mixity. Instead, a single value, $G_c^{\text{int},C}$, is used. The criterion of growth then takes the following expression

$$G^{\text{int},C} = G_c^{\text{int},C}. \tag{70}$$

Although not explicitly indicated, this $G^{\text{int},C}$ is, according to (29), entirely due to mode II. When $G_c^{\text{int},C}$ is relatively small, then according to (62) the crack will continue growing along the interface. It should be pointed out that $G^{\text{int},C}$ evaluated using the contact model has been found smaller than that obtained in the open model, this difference becoming significant for large near-tip contact zones, see Section 7. Only a few experimental works, where some interface crack extension was observed in presence of a detected near-tip contact zone, is known to the present authors, see Liechti and Chai [72, 73] and Banks-Sills and Ashkenazi [8]. Additionally, a measurement of $G_c^{\text{int},C}$ in the presence of physically relevant near-tip contact zones was not an objective of these works.

A question associated to the use of the frictionless model considered up to now arises here, if it is realistic to neglect a possible shielding effect of friction on the crack tip when the near-tip contact zone is relatively large. Note that a difficulty in including friction effects in such an analysis lies in the fact that in this case the singularity order of the near-tip stresses is different from 0.5 when $\beta \neq 0$ (Comninou [20]), being typically less than 0.5, which implies a theoretically vanishing $G_{\mathrm{II}}^{\mathrm{int},C}(\Delta a)$ for $\Delta a \to 0$. This issue has recently been studied by Sun and Qian [126], Qian and Sun [110], Leguillon [70], Audoly [6], and Leblond and Frelat [67]. Sun and Qian [126] and Qian and Sun [110] observed in a numerical study by FEM that this decrease in $G_{\mathrm{II}}^{\mathrm{int},C}(\Delta a)$ was compensated by an increase in the energy dissipated due to friction resulting in a non-zero limit of the energy used for an infinitesimal crack extension. Additionally they showed that, depending on the frictional coefficient, the frictional dissipation energy may constitute a substantial part of the total energy needed for finite crack extensions considered there. A usual approach to solve the 'paradox' with vanishing $G_{\mathrm{II}}^{\mathrm{int},C}(\Delta a)$ is to introduce a material dependent characteristic crack extension length Δa_0 to characterize the interfacial fracture toughness, $G_{\mathrm{II}}^{\mathrm{int},C}(\Delta a_0)$ then being applied in a fracture criterion.

3.2.2.2 Interface crack kinking Taking into account that normal stresses $\sigma_{\theta\theta}^{\mathrm{sing}}$ of the Comninou singular asymptotic stress field are negative for all angles θ directed towards the stiffer material (material 1 for $\beta > 0$), only kink towards the more compliant material is expected. Then, applying conditions (59) to the Comninou asymptotic term of $\sigma_{\theta\theta}^{\mathrm{sing}}(r,\theta)$ in (30), the following expression of θ_{kink}, predicted by MCS criterion is obtained (París *et al*. [103]):

$$\theta_{\mathrm{kink}} = -2\,\mathrm{sgn}(\beta)\arccos\sqrt{\frac{2+|\beta|}{3+|\beta|}} \quad \text{for } \beta \neq 0, \tag{71}$$

where $\mathrm{sgn}(\cdot)$ gives the sign of a real number. Recall that the shear stress component $\sigma_{r\theta}^{\mathrm{sing}}$ vanishes at θ_{kink} given by (71) (see (32)).

The range of the predicted kink angles (mentioned already by Hayashi and Nemat-Nasser [49]) is $64.6^\circ \leq |\theta_{\mathrm{kink}}| \leq 70.5^\circ$. There seems to be a misprint in the kink angle value (16°) predicted by this criterion in Comninou [22], the θ_{kink} here defined associated to this value $90^\circ - 16^\circ = 74^\circ$ being outside of the range for isotropic materials.

It should be stressed that angles θ_{kink} observed in experiments by Comninou [22] agree reasonably well with prediction by MCS criterion.

With reference to the application of MERR, LS and $\mathrm{MK_I}$ criteria a certain kinked crack is required. Now consider a tip of an interface crack with a slipping zone adjacent to the interface crack tip. Let a straight open kink crack of a sufficiently small length b be initiated at this tip. It is expected that after kinking, there will be two adjacent zones along the parent interface crack near its tip, an open zone adjacent to the parent crack tip and a slipping one behind it. The correctness of this assumption has been confirmed by numerical solutions of the corresponding contact problem by FEM in Leblond and Frelat [65, 66] and by BEM in the present work (see Section 7).

A simple and illustrative mechanical explanation, based on the previously discussed Comninou condition $\beta K_{\mathrm{II}}^{C} \geq 0$, of the fact that the kink necessarily deviates towards the softer material, shown schematically at fig. 10, was given by Leblond and Frelat [65, 66].

After the kink, the whole crack is an ordinary one open in the zone adjacent to the tip in a homogeneous material, ordinary SIFs $k_m(\theta_{\mathrm{kink}}, b)$ being associated to this tip ($m = \mathrm{I}, \mathrm{II}$). Limits of

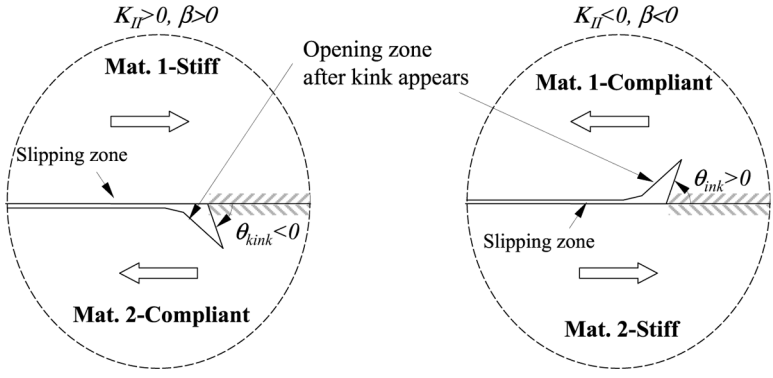

Figure 10: Tendency to open kink crack in two possible situations.

these SIFs for $b \to 0$ can be expressed in a similar way as in (53):

$$k_{\mathrm{I}}(\theta_{\mathrm{kink}}) = C_{12}^{C}(\theta_{\mathrm{kink}}, \alpha, \beta) K_{\mathrm{II}}^{C},$$
$$k_{\mathrm{II}}(\theta_{\mathrm{kink}}) = C_{22}^{C}(\theta_{\mathrm{kink}}, \alpha, \beta) K_{\mathrm{II}}^{C}. \tag{72}$$

Leblond and Frelat [65, 66] have shown that universal dimensionless functions C_{i2}^{C} are functions only of mismatch bi-material parameters, α and β, and kink angle θ_{kink}. Thus, they apply for any situation (geometry of bi-material specimen with crack and load).

According to Leblond and Frelat [65], the coefficients associated to Mode II in (53), and in both (67) and (72) for $\alpha = \beta = 0$ coincide, i.e. $C_{i2}^{h}(\theta) = C_{i2}^{o}(\theta, 0, 0) = C_{i2}^{C}(\theta, 0, 0)$.

MERR, LS and $\mathrm{MK_I}$ criteria may be applied to predict θ_{kink} in an analogous way as done in Sections 3.1.2 and 3.2.1.2. In particular, θ_{kink} predicted by MERR criterion maximizes the energy release rate at an infinitesimal kink:

$$G^{\mathrm{kink}}(\theta) = \frac{k_{\mathrm{I}}^{2}(\theta) + k_{\mathrm{II}}^{2}(\theta)}{E'_{\mathrm{kink}}}. \tag{73}$$

θ_{kink} predicted by LS criterion solves the following implicit equation $C_{22}^{C}(\theta_{\mathrm{kink}}, \alpha, \beta) = 0$, and θ_{kink} predicted by $\mathrm{MK_I}$ maximizes $k_{\mathrm{I}}(\theta)$. As explained above angles θ_{kink} predicted are independent of the loading under the condition of sufficiently large initial near-tip contact zone in the parent crack just before the kink onset. Finally, criteria for kink crack onset take the same form as in (60) and (61).

Recall that, similarly to crack kinking under SSC conditions, θ_{kink} predicted by MCS criterion is independent of α while its prediction by MERR or LS criteria is a function of both mismatch parameters, α and β.

A comparison of θ_{kink} predicted by MCS criterion (71) and LS criterion (computed for some particular bi-materials by FEM in Leblond and Frelat [65, 66]) presented in fig. 11 shows that θ_{kink} predicted by both criteria are only weak functions of mismatch parameters. However, it is somewhat surprising to observe that for $\nu_1 = \nu_2$ and increasing ratio of shear moduli G_1/G_2, angle θ_{kink} predicted by MCS criterion is decreasing while that predicted by LS criterion is increasing. A further analysis of θ_{kink} predictions by all criteria (particularly by MERR, LS and $\mathrm{MK_I}$ that depend on α and β) is required to explain this difference. However, with the exception of experiments carried out by Comninou [22], there are no specific experiments studying cracks kinking from an initially closed interface cracks known to the authors.

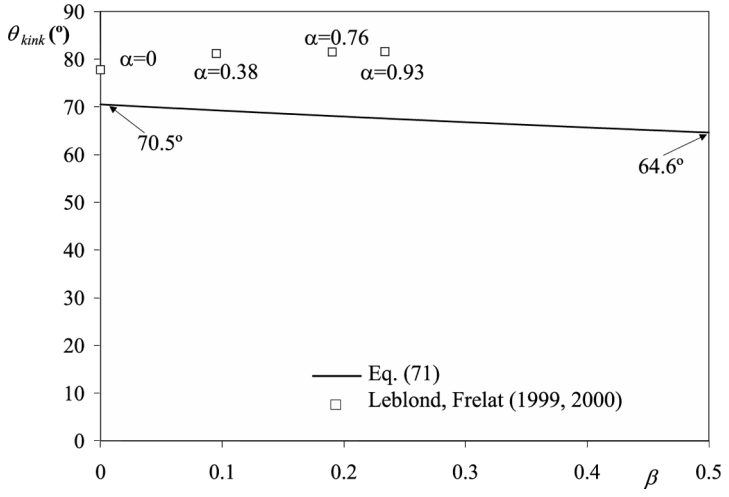

Figure 11: Kink angle θ_{kink} predicted by MCS, eqn (71), and LS (Leblond and Frelat [65, 66]) criteria as a function of β in the contact model.

In situations where during an interface crack growth the contact zone, originally negligible ($r_c \ll r_p$), comes to be physically relevant ($r_c \gg r_p$), the following analysis may be significant in the competition between further crack extension and kinking when this is considered to be governed by (62). Recall that, assuming a sufficiently large contact zone at the parent crack tip in the instant of the kink onset, θ_{kink} predicted by a criterion is fixed, being independent of the problem geometry and loading. Then, taking into account expressions (29) and (73) with (72), $G^{\text{int},C}/G^{\text{kink}}$ is also fixed for a bi-material, being independent of the problem geometry, loading and, in particular, independent of K_{II}^{C}. The implication of this result for the interface crack growth, where the near-tip contact zone length r_c is increasing, is that the crack will not kink, if has not already kinked before a significant contact zone has arisen. In other words, there are no reasons for a crack to kink once the contact model controls the crack extension process. All this considering that the singular term of the Comninou contact model controls the initiation of the kink, the T-stress having no influence in this initiation.

4 BEM for 2D orthotropic elasticity

Boundary element method (BEM), París and Cañas [100] is a numerical method particularly suitable to solve interface crack problems due to the fact that the only elastic variables of the problem (displacements and tractions) which are managed directly are those associated to the boundaries and interfaces of the constituent materials. Several advanced applications of BEM to isotropic and orthotropic (or in general anisotropic) interface crack problems have been developed in the past, see Ang *et al*. [5], Lee and Choi [69], Liu and Feng-Chen [74], Graciani *et al*. [47], Mantič *et al*. [77], Matsumoto *et al*. [83], Paula and Aliabadi [108], París *et al*. [101, 102], Selcuk *et al*. [115], Sládek and Sládek [120], Tan *et al*. [130] and Yuuki and Cho [150], among others.

In this section, first a complex variable formulation of two-dimensional orthotropic elasticity is briefly introduced for the two classes of orthotropic materials, the so-called mathematically non-degenerate and degenerate materials, Ting [132]. Then, a formulation of the Somigliana

displacement and stress identities for plane orthotropic elastic bodies is introduced. Simple explicit formulae in complex variable formulation of all the integral kernels U_{ij}, T_{ij}, D_{ijk} and S_{ijk} and also of the free term coefficient tensor C_{ij} in the Somigliana displacement identity are presented for both classes of orthotropic materials. Finally, a BEM implementation of both Somigliana identities is described.

4.1 Some basic concepts of the complex variable formulation of 2D orthotropic elasticity

The notation used in this section will be closely related to that used in Ting's monograph [132] which presents a comprehensive review of the modern theory of anisotropic elasticity.

Applying the concept of the Airy stress function and using (34), the strain compatibility equation yields the following Lekhnitskii characteristic equation of an orthotropic material [71]:

$$s'_{11}p^4 + (2s'_{12} + s'_{66})p^2 + s'_{22} = 0, \tag{74}$$

whose conjugate roots p_α and $\bar{p}_\alpha$ ($\alpha = 1, 2$) are expressed by:

$$p_\alpha = \frac{\pm s_- + i s_+}{\sqrt{2s'_{11}}}, \tag{75}$$

where $s_\pm$ were defined in (37).

Due to the fact that s_+ is always positive, the imaginary part of p_α can always be taken as positive, $\mathrm{Im}\, p_\alpha > 0$.

A particular class of orthotropic materials with $s_- = 0$, and consequently $p_1 = p_2 = p$, are called mathematically degenerate materials, Ting [132], and will be treated separately from the case of mathematically non-degenerate materials. The most important cases of mathematically degenerate materials are isotropic materials and transversally isotropic materials when the x_3-axis is the symmetry axis. In these particular cases the roots of (74) are $p_1 = p_2 = p = i$.

4.1.1 Mathematically non-degenerate materials

Complex representations of displacements $\mathbf{u}(\mathbf{x})$, tractions $\mathbf{t}(\mathbf{x})$ and stresses $\sigma_{ij}(\mathbf{x})$ ($i, j = x, y$), $\mathbf{x} \in \mathbb{R}^2$, first deduced by Lekhnitskii [71], can be written in terms of analytic functions of complex variables $z_\alpha(\mathbf{x}) = x + p_\alpha y$ and some complex matrices $\mathbf{A}$ and $\mathbf{B}$ introduced by Stroh [122, 123]. Roots p_α of (74) give the eigenvalues and the columns of $\mathbf{A}$ and $\mathbf{B}$ form the eigenvectors of the fundamental elasticity matrix $\mathbf{N}$ in the Stroh formalism of the anisotropic elasticity [132]. The following simple expressions of $\mathbf{A}$ and $\mathbf{B}$ were introduced by Mantič and París [78]:

$$\mathbf{A} = \begin{bmatrix} is_-s_+ - s'_{66}/2 & -(is_-s_+ + s'_{66}/2) \\ -p_1(is_-s_+ + s'_{66}/2) & p_2(is_-s_+ - s'_{66}/2) \end{bmatrix}, \quad \mathbf{B} = \begin{bmatrix} -p_1 & -p_2 \\ 1 & 1 \end{bmatrix}. \tag{76}$$

Note that $\mathbf{A}$ and $\mathbf{B}$ in the above expressions are not normalized in the sense considered in [132].

The Stroh orthogonality relations for anisotropic materials [122, 123] are fundamental for the modern theory of anisotropic elasticity. They reflect the symmetry and positive definiteness of the equations of equilibrium [79] and in the case analyzed can be written as:

$$\mathbf{A}^T\mathbf{B} + \mathbf{B}^T\mathbf{A} = \mathbf{K} = \mathrm{diag}\left[\kappa_1^2, \kappa_2^2\right], \quad \bar{\mathbf{A}}^T\mathbf{B} + \bar{\mathbf{B}}^T\mathbf{A} = \mathbf{0}, \tag{77}$$

where the bar denotes complex conjugate, and the diagonal matrix $\mathbf{K}$ of the normalization coefficients is defined by (see [78]):

$$\kappa_\alpha^2 = 2\sum_{k=1}^{2} A_{k\alpha}B_{k\alpha} = \mp 4is_-s_+p_\alpha \neq 0. \tag{78}$$

Then, the normalized form of $\mathbf{A}$ and $\mathbf{B}$ is obtained by $\mathbf{A}\mathbf{K}^{-(1/2)}$ and $\mathbf{B}\mathbf{K}^{-(1/2)}$.

4.1.2 Mathematically degenerate materials

In the case of a repeated root of (74) the complex representations of displacements, tractions and stresses can be written in terms of analytic functions of complex variable $z(\mathbf{x}) = x + py$ and its complex conjugate $\bar{z}(\mathbf{x}) = x + \bar{p}y$, and the complex matrices $\mathbf{A}$ and $\mathbf{B}$. In the present case the first columns of these matrices form the eigenvector and the second columns the generalized eigenvector of the fundamental elasticity matrix $\mathbf{N}$ in the Stroh formalism. Simple expressions of $\mathbf{A}$ and $\mathbf{B}$ are written as:

$$\mathbf{A} = \begin{bmatrix} -s'_{66}/2 & 2s_+^2 - s'_{66}/2 \\ -ps'_{66}/2 & \bar{p}(2s_+^2 - s'_{66}/2) \end{bmatrix}, \quad \mathbf{B} = \begin{bmatrix} -p & -\bar{p} \\ 1 & 1 \end{bmatrix}. \tag{79}$$

As in the case of non-degenerate materials, expressions of $\mathbf{A}$ and $\mathbf{B}$ presented are not normalized.

The Stroh orthogonality relations write now as:

$$\mathbf{A}^T\mathbf{B} + \mathbf{B}^T\mathbf{A} = \mathbf{K} = \begin{bmatrix} 0 & \kappa^2 \\ \kappa^2 & 0 \end{bmatrix}, \quad \bar{\mathbf{A}}^T\mathbf{B} + \bar{\mathbf{B}}^T\mathbf{A} = \mathbf{0}, \tag{80}$$

where the normalization constant is given as:

$$\kappa^2 = -4s_+^2 p \neq 0. \tag{81}$$

4.2 The Somigliana displacement identity

Let a linear elastic body be defined by an open domain $D \subset \mathbb{R}^2$ with a finite and piecewise smooth boundary ∂D. Starting from the Betti theorem of reciprocity of work and using the concept of concentrated load the Somigliana displacement identity can be derived (e.g. [100]):

$$C_{ij}(\mathbf{x})u_j(\mathbf{x}) + \text{p.v.}\int_{\partial D} T_{ij}(\mathbf{x},\mathbf{y})u_j(\mathbf{y})ds(\mathbf{y}) - \int_{\partial D} U_{ij}(\mathbf{x},\mathbf{y})t_j(\mathbf{y})ds(\mathbf{y}) = 0, \tag{82}$$

where the integral kernels $U_{ij}(\mathbf{x},\mathbf{y})$ and $T_{ij}(\mathbf{x},\mathbf{y})$ respectively are the displacements (weakly singular) and the tractions (strongly singular) at $\mathbf{y}$ originated by the unit-concentrated loads at $\mathbf{x}$. The free-term coefficient tensor $C_{ij}(\mathbf{x}) = \delta_{ij}$ for $\mathbf{x} \in D$, and $C_{ij}(\mathbf{x}) = 0.5\delta_{ij}$ for $\mathbf{x} \in \partial D$ with the exception of the corner points of ∂D. Note that for $\mathbf{x} \in \partial D$ the first integral in (82) is taken in the sense of Cauchy principal value (p.v.) defined by a vanishing circular zone.

Mathematically non-degenerate materials
By application of (77) the following explicit formulae were derived in [78] (see also [81]):

$$U_{ij}(\mathbf{x},\mathbf{y}) = \mathrm{Re}\left\{\sum_{\alpha=1}^{2} \frac{1}{\pi i \kappa_\alpha^2} A_{i\alpha} A_{j\alpha} \log z_\alpha(\mathbf{y}-\mathbf{x})\right\}, \tag{83}$$

$$T_{ij}(\mathbf{x},\mathbf{y}) = \mathrm{Re}\left\{\sum_{\alpha=1}^{2} \frac{1}{\pi i \kappa_\alpha^2} A_{i\alpha} B_{j\alpha} B_{k\alpha} \frac{n_k(\mathbf{y})}{z_\alpha(\mathbf{y}-\mathbf{x})}\right\}, \tag{84}$$

$$C_{ij}(\mathbf{x}) = \mathrm{Re}\left\{\sum_{\alpha=1}^{2} \frac{1}{\pi i \kappa_\alpha^2} A_{i\alpha} B_{j\alpha} \log \frac{z_\alpha^{(1)}(\mathbf{x})}{z_\alpha^{(2)}(\mathbf{x})}\right\}, \quad \mathbf{x} \in \partial D, \tag{85}$$

where $\mathbf{n}(\mathbf{y})$ is the unit outward normal vector to ∂D at $\mathbf{y}$, and $z_\alpha^{(e)}(\mathbf{x}) = r_1^{(e)}(\mathbf{x}) + p_\alpha r_2^{(e)}(\mathbf{x})$, $\mathbf{r}^{(e)}(\mathbf{x})$ are the two unit tangential vectors to ∂D with the origin at $\mathbf{x}$.

Mathematically degenerate materials
By application of (80) the following new explicit formulae, whose deduction is based on the previous work developed in [78, 81], can be derived:

$$U_{ij}(\mathbf{x},\mathbf{y}) = \mathrm{Re}\left\{\sum_{\alpha,\beta=1}^{2} \frac{1}{\pi i \kappa^2} A_{i\alpha} A_{j\beta} G_{\alpha\beta}(z,\bar{z})\right\}, \tag{86}$$

$$T_{ij}(\mathbf{x},\mathbf{y}) = \mathrm{Re}\left\{\sum_{\alpha,\beta=1}^{2} \frac{1}{\pi i \kappa^2} A_{i\alpha} B_{j\beta} (G_{\alpha\beta,z}(z,\bar{z}) B_{k1} + G_{\alpha\beta,\bar{z}}(z,\bar{z}) B_{k2}) n_k(\mathbf{y})\right\}, \tag{87}$$

$$C_{ij}(\mathbf{x}) = \mathrm{Re}\left\{\sum_{\alpha,\beta=1}^{2} \frac{1}{\pi i \kappa^2} A_{i\alpha} B_{j\beta} (G_{\alpha\beta}(z^{(1)}(\mathbf{x}),\bar{z}^{(1)}(\mathbf{x})) - G_{\alpha\beta}(z^{(2)}(\mathbf{x}),\bar{z}^{(2)}(\mathbf{x})))\right\},$$
$$\mathbf{x} \in \partial D, \tag{88}$$

where $z = z(\mathbf{y}-\mathbf{x})$ and $\bar{z} = \bar{z}(\mathbf{y}-\mathbf{x})$,

$$\mathbf{G}(z,\bar{z}) = \begin{bmatrix} \bar{z} z^{-1} & \log z \\ \log z & 0 \end{bmatrix}, \quad \mathbf{G}_{,z}(z,\bar{z}) = \begin{bmatrix} -\bar{z} z^{-2} & z^{-1} \\ z^{-1} & 0 \end{bmatrix}, \quad \mathbf{G}_{,\bar{z}}(z,\bar{z}) = \begin{bmatrix} z^{-1} & 0 \\ 0 & 0 \end{bmatrix}, \tag{89}$$

and $z^{(e)}(\mathbf{x}) = r_1^{(e)}(\mathbf{x}) + p r_2^{(e)}(\mathbf{x})$.

It is an easy matter to verify that in the particular case of isotropic materials the above expressions coincide with the classical ones, see for instance [100].

4.3 The Somigliana stress identity

By differentiation of (82) at $\mathbf{x} \in D$ and application of Hooke's law (34), the Somigliana stress identity can be derived [100]:

$$\sigma_{ij}(\mathbf{x}) + \int_{\partial D} S_{ijk}(\mathbf{x},\mathbf{y}) u_k(\mathbf{y}) ds(\mathbf{y}) - \int_{\partial D} D_{ijk}(\mathbf{x},\mathbf{y}) t_k(\mathbf{y}) ds(\mathbf{y}) = 0, \tag{90}$$

where the integral kernels $D_{ijk}(\mathbf{x},\mathbf{y})$ and $S_{ijk}(\mathbf{x},\mathbf{y})$ respectively are displacements (strongly singular) and tractions (hypersingular) at $\mathbf{y}$ originated by a dislocation dipole (a kind of strain nucleus) at $\mathbf{x}$ [80, 81].

Mathematically non-degenerate materials

The classical direct approach already mentioned to deduce the integral kernels that appear in (90) does not yield simple explicit expressions at these kernels. Simple expression of these kernels can only be obtained for mathematically non-degenerate materials using a symmetrical representation of the stresses [80] as done in [81].

$$D_{ijk}(\mathbf{x},\mathbf{y}) = -\mathrm{Re}\left\{\sum_{\alpha=1}^{2}\frac{1}{\pi i\kappa_\alpha^2}B_{i\alpha}B_{j\alpha}A_{k\alpha}\frac{1}{z_\alpha(\mathbf{y}-\mathbf{x})}\right\}, \tag{91}$$

$$S_{ijk}(\mathbf{x},\mathbf{y}) = \mathrm{Re}\left\{\sum_{\alpha=1}^{2}\frac{1}{\pi i\kappa_\alpha^2}B_{i\alpha}B_{j\alpha}B_{k\alpha}B_{l\alpha}\frac{n_l(\mathbf{y})}{z_\alpha^2(\mathbf{y}-\mathbf{x})}\right\}. \tag{92}$$

Mathematically degenerate materials

By using a procedure analogous to that used in the deduction of (91)–(92) and taking into account the results of Section 4.1.2, (86)–(87) and (89), the following new explicit formulae of D_{ijk} and S_{ijk} have been obtained:

$$D_{ijk}(\mathbf{x},\mathbf{y}) = -\mathrm{Re}\left\{\sum_{\alpha,\beta=1}^{2}\frac{1}{\pi i\kappa^2}B_{i\alpha}(G_{\alpha\beta,z}(z,\bar{z})B_{j1} + G_{\alpha\beta,\bar{z}}(z,\bar{z})B_{j2})A_{k\beta}\right\}, \tag{93}$$

$$S_{ijk}(\mathbf{x},\mathbf{y}) = \mathrm{Re}\left\{\sum_{\alpha,\beta=1}^{2}\frac{1}{\pi i\kappa^2}B_{i\alpha}(G_{\alpha\beta,zz}B_{j1}B_{l1} + G_{\alpha\beta,\bar{z}z}(B_{j2}B_{l1} + B_{j1}B_{l2}))B_{k\beta}n_l(\mathbf{y})\right\}, \tag{94}$$

where

$$\mathbf{G}_{,zz}(z,\bar{z}) = \begin{bmatrix} 2\bar{z}z^{-3} & -z^{-2} \\ -z^{-2} & 0 \end{bmatrix}, \quad \mathbf{G}_{,\bar{z}z}(z,\bar{z}) = \begin{bmatrix} -z^{-2} & 0 \\ 0 & 0 \end{bmatrix}. \tag{95}$$

4.4 Some features of BEM implementation

BEM code applied in the present work solves the Somigliana displacement identity (82) by the standard collocation approach using linear continuous elements in the way described by París and Cañas [100]. Integrals of the products of the integral kernels and the boundary element shape functions can be evaluated analytically or numerically, Avila *et al*. [7]. The advantage of the above complex variable representation of the integral kernels is an easy derivation of the formulae for analytic integrations in the case of linear continuous elements applied. In the present work, all the integrals, regular and singular, have been evaluated analytically.

The removal of the rigid body movements in the case of elastic problems with boundary conditions in tractions is carried out using a procedure based on the Fredholm theory of the boundary integral equations developed in Blázquez *et al*. [10].

The evaluation of stresses inside the domain is performed, once the boundary values of displacements and tractions have been computed, in the postprocessing stage by means of the Somigliana stress identity (90). Here also, all the integrals can be evaluated analytically or numerically.

The adaptation of the present BEM code to the solution of non-linear contact problems will be described in Section 5. Note that the solution of linear multi-domain problems, with perfect interface conditions, is implemented in this code through a particular and simpler variant of the more general contact algorithm.

5 Weak formulation of interface/contact conditions in BEM with non-conforming meshes

Understanding of the contact problem began with the studies of Hertz [52]. Many problems, although usually involving simple geometries and loads and frictionless contact, have been analytically solved since then, Gladwell [45] and Johnson [61]. Nevertheless, numerical methods are required to solve more complicated problems.

The first pioneering works on contact problems using FEM are, among many others, Chan and Tuba [18], Fredriksson [38], Oden and Pires [92] and Okamoto and Nakazawa [93]. In BEM, some of the pioneer works are Andersson [4], Man *et al*. [76], París and Garrido [104, 106] and París *et al*. [107]. All of them use identical meshes in the zones of the bodies candidate for contact, establishing the contact conditions between the corresponding pair of nodes. Later, algorithms in which the contact conditions are established between non-conforming meshes arise. These algorithms simplify significantly the preparation work of the meshes and also permit more complex problems to be considered (e.g. with large displacements). The first non-conforming algorithms, Bathe and Chaudhary [9] and Klarbring and Bjorkman [62] in the field of FEM and Blázquez *et al*. [11], Huesmann and Kuhn [55] and Olukoko *et al*. [94] in the field of BEM, extrapolate the ideas of conforming meshes and establish the contact conditions between nodes and intermediate points of the elements, using a scheme that can be called strong imposition or node-to-point scheme of application of contact conditions. Blázquez *et al*. [14] investigated the problems that might arise with this scheme of application of the contact conditions and developed a scheme called weak approach, Blázquez *et al*. [15], that avoided the problems found with the former scheme. This weak approach of application of contact conditions will be followed in this chapter.

5.1 Contact conditions

Let us assume (fig. 12) two 2D bodies, A and B, occupying the domains D^A and D^B with boundaries ∂D^A and ∂D^B, which interact between them through a common contact zone $\partial D_c^A = \partial D_c^B = \partial D_c$. The loads, which are assumed to depend on a parameter λ, are given by the tractions and displacements prescribed along the boundaries ∂D_t^K, ∂D_u^K and ∂D_{ut}^K respectively, $\partial D_t^K + \partial D_u^K + \partial D_{ut}^K = \partial D_l^K = \partial D^K - \partial D_c^K$, $K = A, B$. Thus, the boundary conditions of the problem along ∂D_l^K are expressed as:

$$\begin{aligned} u_i^K &= \bar{u}_i^K(\lambda), \quad \text{along } \partial D_u^K, \quad i = 1,2, \quad K = A,B, \\ t_i^K &= \bar{t}_i^K(\lambda), \quad \text{along } \partial D_t^K, \quad i = 1,2, \quad K = A,B, \\ u_i^K = \bar{u}_i^K(\lambda),\ t_j^K &= \bar{t}_j^K(\lambda), \quad \text{along} \partial D_{ut}^K, \quad i,j = 1,2, i \neq j, \quad K = A,B, \end{aligned} \tag{96}$$

Directions i can be associated to any cartesian system of reference, although typically they are referred to a local system used for contact conditions that will be defined in that which follows.

Contact conditions are established in a normal-tangential coordinate system and are classified in three groups: equilibrium (97), compatibility of normal displacements (98) and, assuming

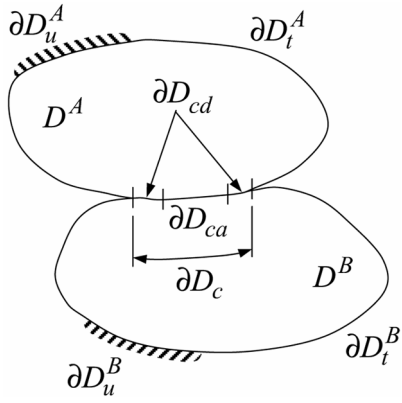

Figure 12: The contact problem.

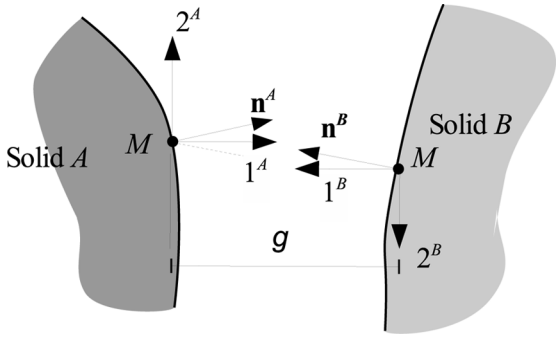

Figure 13: The contact coordinate system.

frictionless case, zero tangential stress (99). For a point M that belongs to the contact zone, these conditions are established with reference to a local system where axis 1^K is the outward normal to ∂D^K and axis 2^K is anticlockwise tangent to ∂D^K. In the numerical solution of contact problems, due to the fact that the outward normals to the two contacting solids may not coincide, it is necessary to define a common system of coordinates in which the former contact conditions and their corresponding checking are carried out. The system used here defines (fig. 13) at each point M of the contact zone, direction 1 as the average of the two outward normals to the boundaries (n^A, n^B), direction 2 being perpendicular to direction 1 and anti-clockwise.

- Equilibrium:
$$t_i^A(M) = t_i^B(M) \leq 0, \quad i = 1, 2, \tag{97}$$
where the compression character of the contact tractions has been explicitly shown.
- Compatibility of normal displacements:
$$u_1^A(M) + u_1^B(M) = g, \tag{98}$$
g being the gap that exists between the surfaces of the bodies at point M.
- Tangential stresses are null:
$$t_2^K(M) = 0, \quad K = A, B. \tag{99}$$

In the case of bonded boundaries the conditions that must be applied are (97) and (98), taking into account that the gap is null and the normal stresses can be tensions. The condition of null shear stress (99) must be replaced by the compatibility of tangential displacements:

$$u_2^A(M) + u_2^B(M) = 0. \tag{100}$$

5.2 Weak formulation of contact conditions

Following the basic idea of imposition of the contact conditions with non-conforming discretizations, described by París *et al*. [97], compatibility equations will be imposed on one of the bodies whereas equilibrium equations will be imposed on the other body.

5.2.1 Compatibility

Two fields of displacements, (101) and (102), will be defined in order to apply compatibility conditions on body A.

$$u_i^A(\mathbf{x}), \forall \mathbf{x} \in D^A \implies \text{displacement solution of body } A, \tag{101}$$

$$u_i^{\partial A}(\mathbf{y}), \forall \mathbf{y} \in \partial D^A \implies \begin{cases} u_i^A(\mathbf{y}) & \text{along } \partial D_l^A, \\ -u_i^B(\mathbf{y}) + \delta_i(\mathbf{y}) & \text{along } \partial D_c^A. \end{cases} \tag{102}$$

Notice that the displacement field $u_i^A(x)$, which corresponds to the solution of the problem, is defined at all points of body A, and will have associated a compatible strain field $\varepsilon_{ij}^A(x)$, whereas $u_i^{\partial A}(y)$ is only defined at points on the boundary. Note that the physical meaning of the variable $\delta_1(y)$ that appears in (102) is the value of how close or how far the boundaries get at point y, whereas $\delta_2(y)$, also in (102), represents the relative displacement between the two surfaces at point y.

To establish compatibility between these two fields of displacements, the principle of virtual forces (i.e. the principle of virtual work where the stress field is a virtual field in equilibrium and the displacement and strain fields correspond to the actual problem) is applied. This principle, for the case of the absence of body forces, takes the expression:

$$\int_{D^A} \sigma_{ij}^{A\psi}(\mathbf{x}) \varepsilon_{ij}^A(\mathbf{x}) dv = \int_{\partial D^A} t_i^{A\psi}(\mathbf{y}) u_i^{\partial A}(\mathbf{y}) ds, \tag{103}$$

an expression that must be satisfied for every virtual field of stresses $\sigma_{ij}^{A\psi}$ and $t_i^{A\psi}$ in equilibrium.

According to [15] it follows that, for the displacement fields defined in (101) and (102) to be compatible:

$$\int_{\partial D_c^A} t_i^{A\psi}(\mathbf{y}) \Big(u_i^A(\mathbf{y}) + u_i^B(\mathbf{y}) - \delta_i(\mathbf{y}) \Big) ds = 0. \tag{104}$$

Expressing eqn (104) in an approximate form, according to the discretization performed, and taking into account that (104) must be fulfilled for any field $t_i^{A\psi}$ in equilibrium:

$$\sum_k^{NCA} \int_{\partial D^{kA}} \left(\mathbf{N}^{kA} \right)^{\mathrm{T}} \mathbf{N}^{kA} ds \mathbf{u}_i^{kA} + \sum_k^{NCA} \int_{\partial D^{kA}} \left(\mathbf{N}^{kA} \right)^{\mathrm{T}} \mathbf{N}^B ds \mathbf{u}_i^B - \sum_k^{NCA} \int_{\partial D^{kA}} \left(\mathbf{N}^{kA} \right)^{\mathrm{T}} \mathbf{N}^{kA} ds \mathbf{d}_i^k = 0, \tag{105}$$

where *NCA* is the number of elements of the body *A* which belong to the potential contact zone and the superindex *k* makes reference to the element of *NCA* along which the integration is performed, **N** are matrices that contain the shape functions of the corresponding elements, **u** are vectors that contain the displacements of the bodies and **d** is a vector that contains the relative normal and tangential displacements between the two surfaces of the bodies at each node of *A*. Note that the shape function matrix $\mathbf{N}^B$ has been kept complete due to the fact that an element of *A* will not necessarily contact with a single element of *B* and *vice versa*.

The computation of the integrals that appear in (105) is commented on in detail in [15]. That multiplying to $\mathbf{u}_i^{kA}$ and $\mathbf{d}_i^k$ only depends on the length of the element *k* of body *A*, being independent of the relative positions of the nodes of both bodies. With reference to that multiplying to $\mathbf{u}_i^B$, it depends on the relative positions in which the nodes of *B* are situated along the element *k* of *A*.

5.2.2 Equilibrium

Analogously to compatibility, two stress states will be defined for the body *B*:

$$t_i^B(\mathbf{x},\mathbf{n}) = \sigma_{ij}^B(\mathbf{x})n_j, \quad \forall \mathbf{x} \in D^B \implies \text{stress solution of body } B, \tag{106}$$

$$t_i^{\partial B}(\mathbf{y}), \quad \forall \mathbf{y} \in \partial D^B \implies \begin{cases} t_i^B(\mathbf{y},\mathbf{n}^B) & \text{along } \partial D_l^B, \\ t_i^A(\mathbf{y},\mathbf{n}^B) & \text{along } \partial D_c^B, \end{cases} \tag{107}$$

where $\mathbf{n}$ is an arbitrary unit vector and $\mathbf{n}^K$ is the outward unit normal to the boundary of body *K* at point *y*.

Notice again that $t_i^B(\mathbf{x},\mathbf{n})$ is defined on the whole of body *B*, whereas $t_i^{\partial B}(\mathbf{y})$ is only defined along the boundary of body *B*.

Applying now the principle of virtual displacements (i.e. the principle of virtual work where the displacement and strain fields are virtual compatible fields and the stress field corresponds to the actual problem), it must be fulfilled, in order to guarantee the equilibrium between these two stress fields, that:

$$\int_{D^B} \sigma_{ij}^B(\mathbf{x})\varepsilon_{ij}^{B\psi}(\mathbf{x})dv = \int_{\partial D^B} t_i^{\partial B}(\mathbf{y})u_i^{B\psi}(\mathbf{y})ds, \tag{108}$$

for any field of displacements $u_i^{B\psi}$ and compatible strains $\varepsilon_{ij}^{B\psi}$.

According to [15], performing similar operations to those indicated for the compatibility equation, the following equation system is obtained:

$$\sum_k^{NCB} \int_{\partial D^{kB}} \left(\mathbf{N}^{kB}\right)^{\mathrm{T}} \mathbf{N}^{kB} ds \mathbf{t}_i^{kB} - \sum_k^{NCB} \int_{\partial D^{kB}} \left(\mathbf{N}^{kB}\right)^{\mathrm{T}} \mathbf{N}^A ds \mathbf{t}_i^A = 0. \tag{109}$$

The integrals that appear in these equations are similar to those that appeared in the compatibility equations and they are computed in a similar way.

It should be noticed that this manner of imposing the equilibrium equations ensures the global equilibrium of forces and moments of the problem. Obviously, the finer the discretization used for $u_i^{B\psi}(\mathbf{y})$, the more similar the values of tractions at points of the two bodies obtained from the system of equations (109) will be.

5.2.3 Frictionless condition

As has been commented previously, in this chapter only the frictionless case is considered, $t_2^K(\mathbf{y}) = 0$. Due to the fact that these conditions affect the stresses, they must be imposed on

the nodes of body A, which controls the stresses along the contact zone. Then:

$$\mathbf{t}_2^A = \mathbf{0}. \tag{110}$$

The system of equilibrium equations (109) translates this condition to the boundary of the solid B.

5.3 Stability conditions

In order to guarantee the correct use of non-conforming meshes a study on the influence of the non-conformity on the results has to be performed. Using BEM, the errors may be more significant in the stresses and appear more frequently in problems with friction. In [12, 97] it is concluded that the results are substantially better if more elements are in the body that controls the displacements: $NCB \gg NCA$, a conclusion confirmed in later publications by these authors.

With reference to this point, a particular study is performed in [13] to detect the errors that appear as a function of the relative position of the point where the node of A contacts the element of B. The conclusion of this work is that the degree of conformity (or unconformity) of a discretization is directly related to the relative distance from the nodes of the body that controls the stresses to the nodes of the discretizations of the body that controls the displacements, and not to the relative size of the elements of the meshes of both solids. The lesser this distance the smaller the errors introduced, and this distance decreases if there are many more nodes controlling displacements.

This problem is inherent to the non-conforming character of the discretizations and it is more severe in node-to-point approaches, but it also appears, although to a much lesser extent, in a weak approach.

5.4 Incremental approach

In frictionless problems the final solution is not dependent on the path and the problem can be solved in one increment of load once, after an iterative procedure, a correct solution (compatible and in equilibrium) is reached. The dissipative character of the friction resulted in an incremental procedure following the evolution of the load being required in the presence of friction.

With reference to the frictionless case, the non-lineal character of the problem comes from the possible variations in the extent of the contact zone with the application of load. The increase in the size of the contact zone is detected checking the interpenetrations in the zone free of contact. The decrease in the size of the contact zone is detected checking the presence of tensions in the contact zone. These checks are performed at the nodes of solid A (which controls the stresses), due to the fact that it is in them that the relative normal displacements (102) and the stresses appear.

Although an iterative procedure would be applicable for the frictionless case under consideration, an incremental procedure will be applied here due to the fact that it is the general approach used by the authors for all contact cases including friction, see [104, 106] for conforming meshes and [97, 15] for the details associated to non-conforming meshes. Due to this general purpose of the approach followed, all the equations will be presented in incremental form.

Let us assume that after a certain application of load the i-th increment starts with a certain set of contact conditions. The system of equations to be solved in this increment of load is constituted by:

- The set of integral equations corresponding to the two bodies involved in the contact, equations (82) in incremental form.
- Compatibility equations corresponding to the potential contact zone, applied to one of the bodies, called body A, equations (105) in incremental form.

- Equilibrium equations corresponding to the potential contact zone, applied to the other body, called body B, equations (109) in incremental form.
- The condition of free stress surface must be imposed at all the nodes n that belong to the potential contact zone of body A but are not in contact:

$$\Delta t_1^A(n) = 0, \quad \Delta t_2^A(n) = 0. \tag{111}$$

- In nodes of body A that are in contact, the conditions:

$$\Delta \delta_1(n) = 0, \quad \Delta t_2^A(n) = 0, \tag{112}$$

must be applied.
- Finally, in nodes of body A that are in a bonded interface, the conditions:

$$\Delta \delta_1(n) = 0, \quad \Delta \delta_2(n) = 0, \tag{113}$$

must be applied.

The remaining load is applied (in fact any value can be applied because what is interesting to detect is the evolution of the solution with the load), and the adequate increment of load must be determined once the system has been solved. In frictionless cases two possible limits of application of the contact conditions are checked, thus detecting the fraction of load λ_j ($0 \leq \lambda_j \leq 1$, $j = 1, 2$) for which the end of linear behavior for each type of condition is reached. The maximum admissible increment of load that can be applied is defined by the value $\lambda = \min(\lambda_j)$, these λ_j being associated to the following situations:

1. Reduction of the contact zone, originated by the appearance of tractions at a node, n, of body A:

$$t_1^A(n)_{i-1} + \Delta t_1^A(n) > 0. \tag{114}$$

The correct value of λ_1 is calculated identifying the final value of the normal stress in (114) with zero.

$$t_1^A(n)_i = t_1^A(n)_{i-1} + \lambda_1 \Delta t_1^A(n) = 0 \implies \lambda_1 = -\frac{t_1^A(n)_{i-1}}{\Delta t_1^A(n)}. \tag{115}$$

The node will be moved, after the application of this increment of load, from ∂D_c^A to ∂D_t^A. The situations described here can obviously arise at several nodes, the value of λ_1 defined by (115) being the minimum of all.

2. When there are nodes of A that trespass the boundary of body B, this means an increase in the size of the contact zone. Under the hypothesis of small displacements, it is normal to work with a gap associated to each node of body A (for instance the distance, projected on the normal, from the node of A to the corresponding point of the boundary of body B). The fraction of load that must be applied is that which makes the gap zero:

$$g(n)_i = g(n)_{i-1} + \lambda_2 \delta_1(n) = 0 \implies \lambda_2 = -\frac{g(n)_{i-1}}{\delta_1(n)}. \tag{116}$$

After the application of the increment of load the node will pass from ∂D_t^A to ∂D_c^A.

After an increment of load the geometry (and consequently the integration constants) may be updated, allowing the consideration of situations different from those covered by the small displacement theory.

6 BEM analysis of delamination in 0°/90° laminate

The presence in a laminate of laminas oriented 90° with respect to the preferred direction of load generates almost immediately the appearance in these laminas of cracks transversal to the load (parallel to the fibers in the lamina). These cracks reach the interface with the neighboring lamina, which is usually oriented 0°. This can originate the bifurcation of the crack, which appears to be propagating as a delamination crack between the two laminas. The stress states that appear at the neighborhood of the tips of the transversal cracks terminating at an interface and of the tips of the interface cracks are very complex and have attracted the attention of a great number of authors (see for instance Ang *et al*. [5], Hwu and Hu [58], Tewary and Kriz [131] and Ting and Hoang [134], among others). The length of the delamination crack, oriented parallel to the load, may originate the appearance of contact between the crack faces. Each lamina can be modeled, considering it from a macroscopic point of view, as a homogeneous orthotropic material subjected to a generalized plane strain state.

The laminate under consideration in this study is a $[0_m,\ 90_n]_S$ under tension as described in fig. 14. A crack transversal to the load is present in the 90° lamina. Due to the symmetry, only one fourth of the problem requires to be studied.

Material characteristics of both laminas are as follows, direction 1 corresponding to the fiber direction: $E_{11} = 45.6\,\text{GPa}$, $E_{22} = E_{33} = 16.2\,\text{GPa}$, $\nu_{12} = \nu_{13} = 0.278$, $\nu_{23} = 0.4$, $G_{12} = G_{13} = 5.83\,\text{GPa}$, $G_{23} = 5.786\,\text{GPa}$.

The load is defined by a displacement, $u_y = 0.02\,\text{mm}$, imposed at the top side, and a generalized plane strain state, with a transversal strain applied of $\varepsilon_{zz} = -0.001258$ which corresponds to the application of a nominal elongation of $\varepsilon_{yy} = 0.01$ for the undamaged material, is assumed in both laminas.

6.1 Stress State at the neighborhood of the crack tip

In Mantič *et al*. [77] a detailed study of the stress state that appears at the neighborhood of the delamination crack of this specimen for a length of $L = 2\,\text{mm}$ is performed. Results corresponding to this problem and $d/L = 0.1$ are shown in fig. 15. The dashed line that appears in the graph corresponding to σ_{xx} represents the values obtained for the case in which the transversal crack is complete and there is no delamination crack, $d = 0$.

Two comments are appropriate with reference to the understanding of the results obtained [77]:

- At the neighborhood of the interface crack tip very high and localized values of normal stresses σ_{xx} are obtained, which apparently have singular character. It is worth observing that these values correspond to tension, while this area is placed in a zone where nominal stresses are given by compression (understanding as nominal the values obtained for the case $d = 0$ taken as reference and included in fig. 15. A detail of this distribution of σ_{xx} in the zone discussed is shown in fig. 16.
- In agreement with the distribution of stresses σ_{xx} at the neighborhood of the interface crack tip, where there is a zone with zero stresses, a separation of boundaries of both laminas appears. The appearance of this bubble has already been explained in Section 2.1.2 (see fig. 4). The morphology of the bubble numerically computed, shown in fig. 17, is absolutely similar to that predicted by analytical studies of interface cracks between isotropic materials carried out by Comminou and Schmueser [24] and Gautesen and Dundurs [41].

The actual situation, in accordance with the discretization performed (as will be seen, more extremely refined discretizations would not produce more useful information from a Fracture

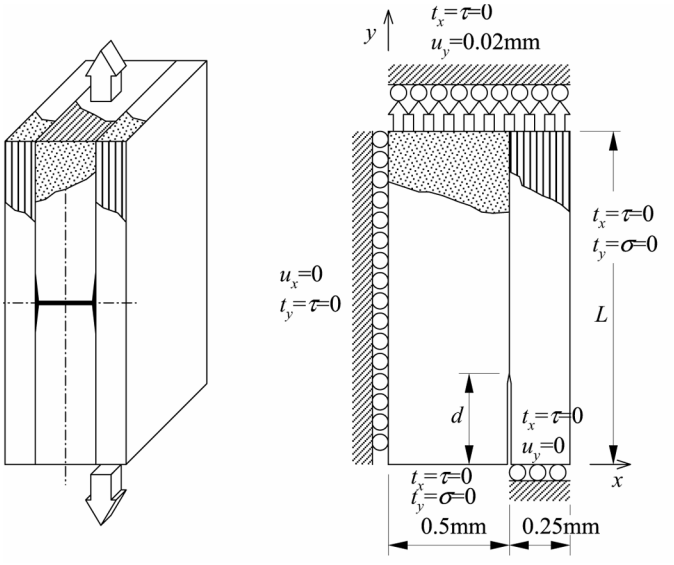

Figure 14: Configuration of the problem.

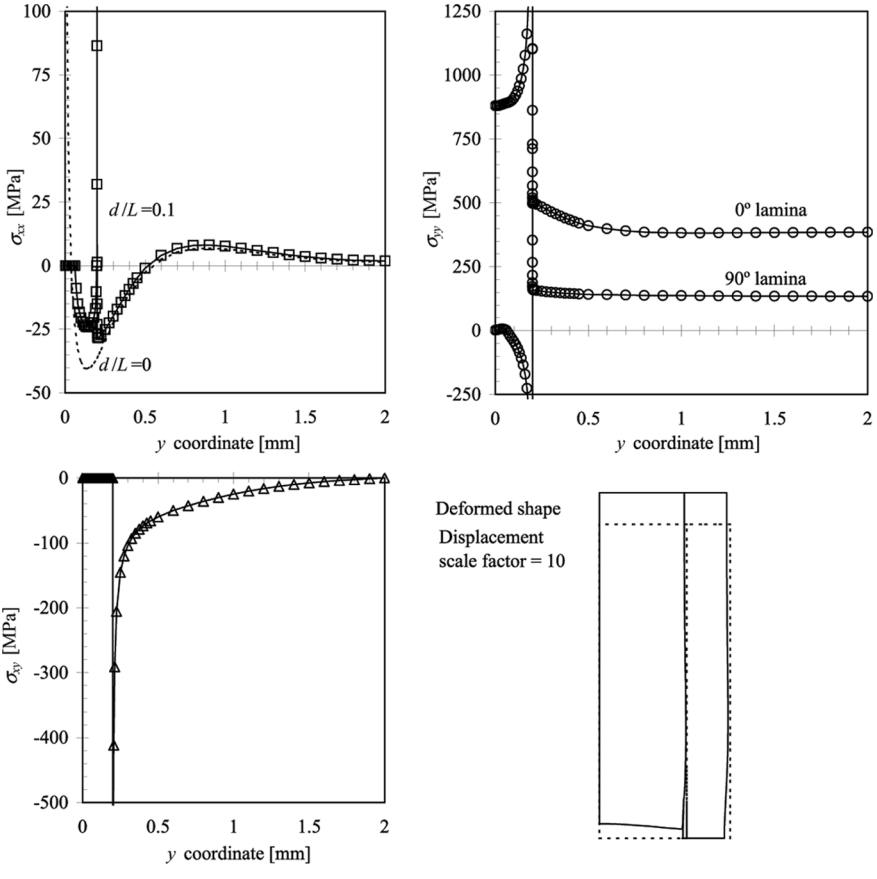

Figure 15: Results for $L = 2$ mm and $d/L = 0.1$.

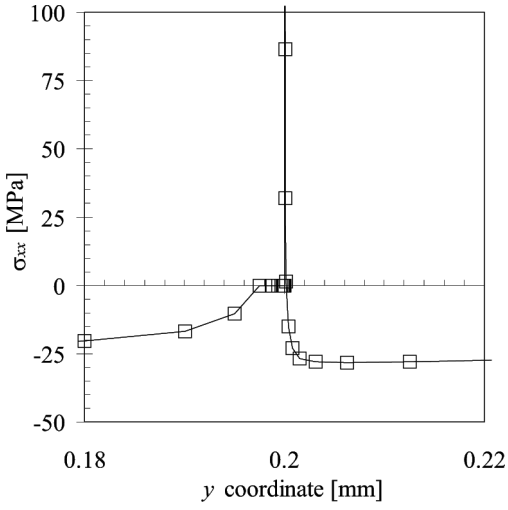

Figure 16: σ_{xx} at the crack tip ($d/L = 0.1$).

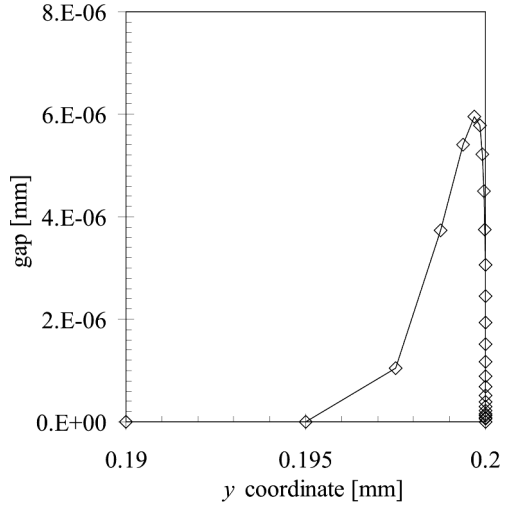

Figure 17: Gap at the crack tip ($d/L = 0.1$).

Mechanics point of view), is the following. The near-tip contact zone predicted by the contact model has not been found in the BEM analysis performed due to the fact that the estimated size of this zone, of an order of 10^{-70} mm, is not detectable by the discretization carried out. In view of this extremely small size of the near-tip contact zone predicted, the small-scale contact (SSC) conditions are fulfilled, the open model being adequate for an analysis of the delamination crack growth. Consequently, a singular distribution of both traction components, σ_{xx} (that is bounded in the contact model of the interface cracks, Section 2.1.2) and σ_{xy}, has been obtained.

In [77] it is shown that, although the distribution of the stresses along the interface, at the neighborhood of the crack tip, is qualitatively similar for any delamination crack, for the cracks with length smaller than $d = 0.1$ mm (one half of that here presented but significantly greater than 0.005 mm which is the size of the bubble for $d = 0.2$ mm), there is no finite contact zone.

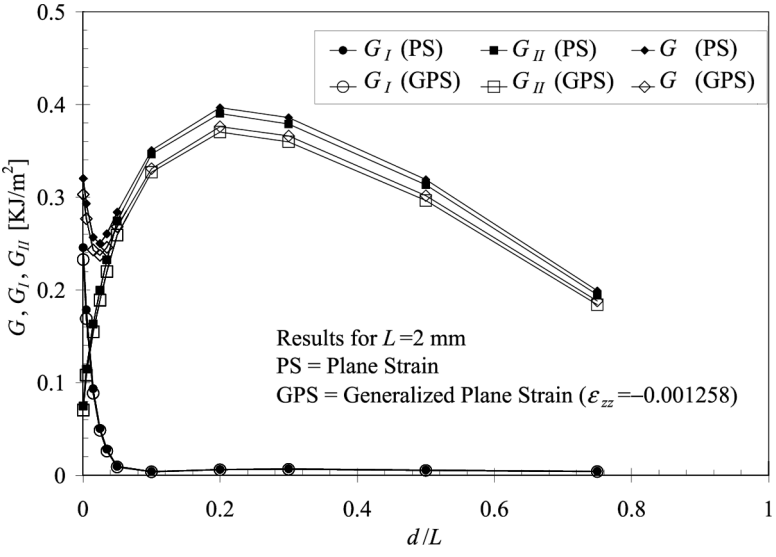

Figure 18: Values of the ERR G as a function of d/L for the configuration of plain strain and generalized plain strain.

Consequently, the whole delamination crack appears to be open. In contrast, for greater lengths of the delamination crack (as for the size here considered) there is always a finite contact zone (separated from the crack tip by a bubble) whose appearance is basically due to the Poisson effect of the 90° lamina.

6.2 Energy release rate of the delamination crack

Figure 18 represents the evolution of the ERR by a delamination crack as a function of its size. The two parts of the ERR corresponding to Modes I and II have been separately represented. The upper index 'int' (used in Sections 2 and 3) has here been omitted from ERR values because it is not ambiguous in this section, where kinking is not considered.

It can be observed that except for small lengths of delamination the growth will be controlled by Mode II, which is obviously coherent with the relative orientation of the crack with respect to the load. Nevertheless, it is quite significant for the generation and progression of the crack in the earlier state that the dominant mode is I due to the smaller value of the fracture toughness associated to this mode.

In fig. 18 the results corresponding to the plane strain case have also been included in order to compare them with those corresponding to generalized plain strain. It can be observed that the results corresponding to the two models are for this particular case qualitatively similar and only differ slightly from a quantitative point of view.

In accordance with the evolution of the ERR G with the delamination, it is suggested that there is a period of stable initiation of the crack (dominated by Mode I), followed by another period of unstable crack growth (up to a length of 20% of L, $d = 0.4$ mm, in the configuration studied). Finally, a period of stable growth, consistent with the fact that G must tend to zero when d tends to L, appears.

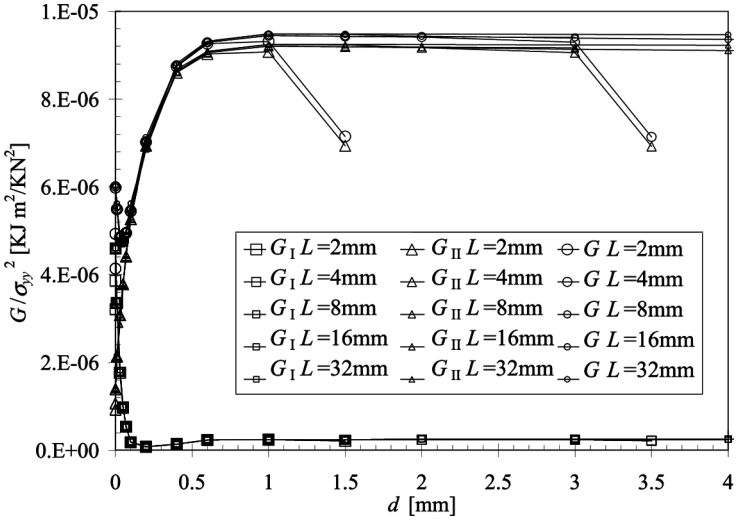

Figure 19: Comparison of the values of G normalized by effective stress for different delamination cracks.

Figure 19 shows the influence of the length of the specimen on the evolution of the ratio G/σ_{yy}^2 versus d, σ_{yy} being the average stress applied. From the figure it is clearly noticeable that the functional dependence of G on σ_{yy} has the form:

$$G = \sigma_{yy}^2 F(d). \tag{117}$$

An immediate consequence of this relation is its lack of dependence on the length of the specimen. The points that appear in the figure out of the plateau value correspond to the natural evolution of G on d when the crack approaches the end of the specimen ($L = 2$ mm and $L = 4$ mm in the figure). The fact of having found a plateau value of G/σ_{yy}^2 is related to the results obtained analytically for a specimen of infinite length by O'Brien [91], using a very simple model. The value obtained using an O'Brien model for the case under consideration is $G/\sigma_{yy}^2 = 1.09 \times 10^{-5}\text{kJ} \times \text{m}^2/\text{kN}^2$, whereas the value numerically obtained is $G/\sigma_{yy}^2 = 0.94 \times 10^{-5}\text{kJ} \times \text{m}^2/\text{kN}^2$.

6.3 Concluding remarks

The stress state found at the neighborhood of the crack tip for different lengths of the delamination crack is qualitatively independent of the length of the crack. Once a certain significant length of the crack is reached, a finite contact zone separated from the crack tip by a bubble appears. Thus, the characteristic singular behavior (associated to the open model of interface cracks) of both, normal and tangential, stresses takes place ahead of the delamination crack tip.

If the test is displacement controlled (fig. 18) the study of the ERR of the delamination crack shows that there is initially an evolution of ERR with the delamination length under mixed mode, an evolution which is independent of the length of the specimen. Sizes at which this behavior appears are very small and of questionable application for Fracture Mechanics considering the plies as homogeneous. The length of the crack at which Mode I disappears is comparable to a length at which Fracture Mechanics can be applied, the growth of the crack being from this moment under pure Mode II.

7 BEM analysis of propagation of fiber/matrix interface crack subjected to transversal load

Under loads normal to the direction of the fibers, composites suffer failures that are known as matrix or inter-fiber failures, typically involving interface cracks between matrix and fibers, the coalescence of which originates macrocracks in the composite, as shown in fig. 20. The purpose of this section is to develop a micromechanical model, using the BEM, to generate information aiming to explain and support the mechanism of appearance and propagation of the damage. To this end, a single fiber surrounded by matrix and with a partial debonding is considered in this study.

A scheme of the micromechanical view of the failure is represented in fig. 21, where all stresses that might have any influence in the failure, París *et al*. [102], appear, though only σ_{22} is considered in this study. In particular, in fig. 21(a) the failure at a plane in an idealized configuration of a fibrous composite is presented, a failure along a vertical plane being assumed in this case. This failure at micromechanical level involves, as a first step of the mechanism of damage, the presence of a crack running between the fiber and the matrix as is indicated in fig. 21(b). The second step of the mechanism includes the kinking of the crack, once it has grown to a certain extension in the interface, then continuing its propagation through the matrix and coalescing with other cracks, then giving rise to a macrocrack.

This exercise is divided into two parts corresponding to both steps of the mechanism of failure. In the first one the circumferential interface crack between the fiber and the surrounding matrix is considered (Section 7.2). In the second one the kink and penetration of the crack into the matrix is considered (Section 7.3).

7.1 The BEM model

The geometry of the target problem appears in fig. 22. Results for the first step of the mechanism of damage under study, that is, the propagation of the crack along the interface, are obtained using a model where boundaries corresponding to the kinked crack are not considered, a similar configuration having already been studied by París *et al*. [101]. The BEM model employed considers the possibility of the appearance of a contact zone and makes use of linear continuous elements. To characterize the problem from the Fracture Mechanics point of view, the ERR for a determined debonding θ_d is used:

$$G^{\text{int}}(\theta_d) = \lim_{\delta \to 0} \frac{1}{2\delta} \int_{\theta_d}^{\theta_d+\delta} \left\{ (\sigma_{rr})_{\theta_d} (\triangle u_r)_{\theta_d+\delta} + (\sigma_{r\theta})_{\theta_d} (\triangle u_\theta)_{\theta_d+\delta} \right\} d\theta, \tag{118}$$

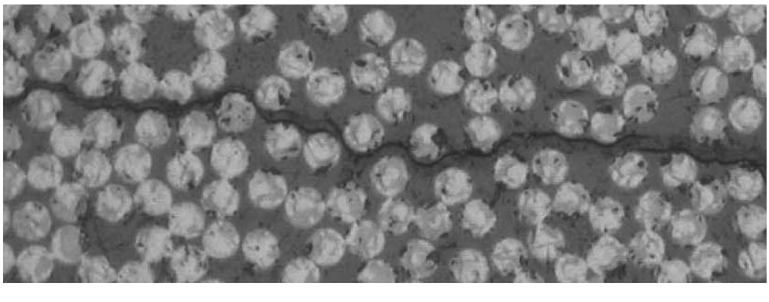

Figure 20: Matrix/inter-fiber failure.

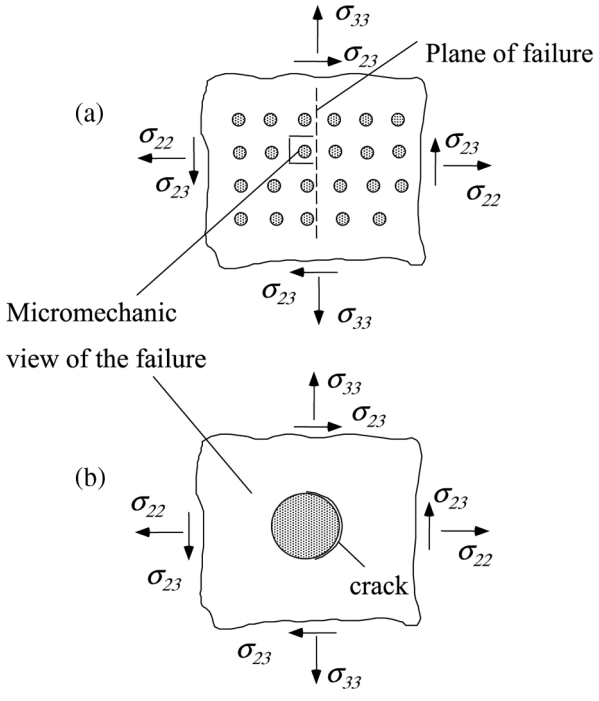

Figure 21: Micromechanical scheme of the matrix/inter-fiber failure.

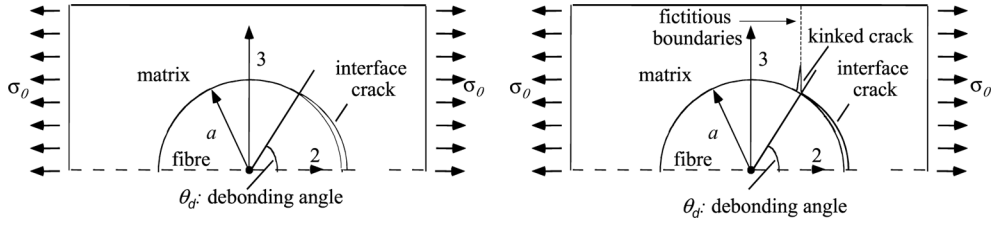

Figure 22: The single fiber model employed.

where σ_{rr} and $\sigma_{r\theta}$ represent respectively radial and shear stresses along the interface and $\triangle u_r$ and $\triangle u_\theta$ their associated relative displacements, θ_d being the angle of the crack.

All results have been obtained for a glass-epoxy system of properties: $\nu^f = 0.22$, $\nu^m = 0.33$, $G^f = 29 \times 10^9$ Pa, $G^m = 1.05 \times 10^9$ Pa, $a = 7.5 \times 10^{-6}$ m.

7.2 The interface crack

In this section the first part of the mechanism of damage under study, i.e. the evolution of the crack along the interface, is studied. Three aspects have been considered here to be the main ones in the study of the interface crack: the origin of the contact zone that appears between both lips of the interface crack, the character of the stresses at both sides of the crack tip and the evolution of the ERR as the crack grows along the interface.

7.2.1 Contact zone size

In order to understand the evolution of the contact zone as the crack grows along the interface, knowledge of the origin of the appearance of the contact zone is required. Two reasons were mentioned by París *et al*. [101] to explain the appearance of this contact zone. One was the change in the relative orientation of the end of the crack, when the crack grows, with respect to the direction of the applied load. The other reason was the already mentioned fact, demonstrated by Comninou [19], that there is always a contact zone in a crack between dissimilar materials. The existence of this contact zone is independent of the presence of normal or tangential stresses, although the size of the contact zone is a very small fraction of the crack length in the presence of normal stresses and the contact zone can reach a significant part of the crack length under tangential stresses.

To clarify the contribution of these effects to the appearance of the contact zone (the connection with the type of growth of the crack will be studied later), the case of dissimilar materials studied in [101] will be compared here with the case of similar materials using the properties of the matrix. The applicability of the Comninou effect is restricted to the case of cracks between dissimilar materials. Thus, studying the same configuration but with the same properties for both the matrix and the fiber, the appearance of the contact zone should only be caused by the load orientation effect.

Figure 23 shows the evolution of the contact zone versus the size of the crack, for both cases, fiber and matrix and similar materials. A meaningful delay is observed in the appearance of the contact zone for the case of similar materials with respect to the case of dissimilar materials. This appearance, for similar materials, takes place for a debonding angle of 77°, the code having detected, with the discretization performed, no contact up to that point. This result is in excellent agreement with Muskhelishvili solution [90] which gives 76.9884°. Thus, it can be deduced that all contact appearing for debondings lower than 77°, for dissimilar materials, must be due to the Comninou effect in either of its two variants, first caused by the normal stress when the crack is very small and later leading to detectable size when large tangential stresses appear. From 77° on, the effect of the orientation of the load is added to the former ones.

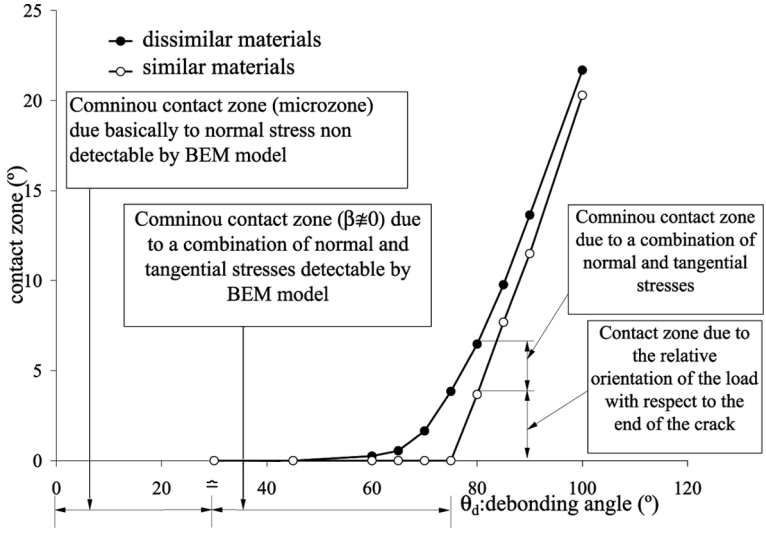

Figure 23: Contact zone evolution versus debonding angle.

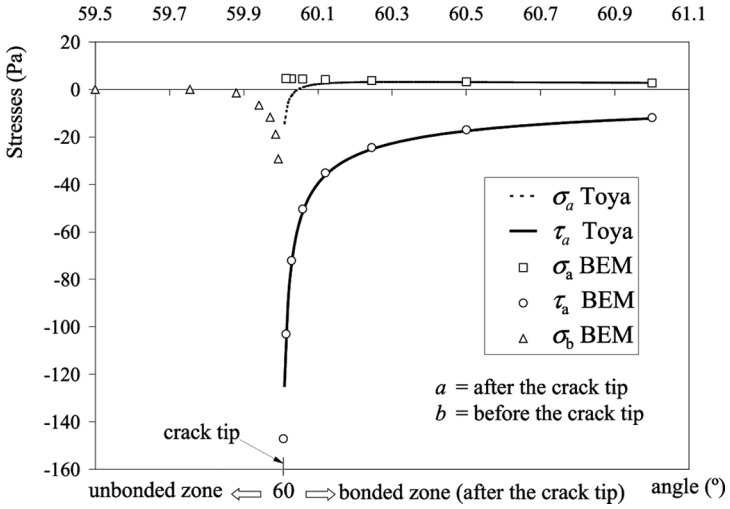

Figure 24: Character of stresses at both sides of the crack tip for θ_d=60°.

7.2.2 Study of the stresses character at both sides of the crack tip

For the case of dissimilar materials, the appearance of the contact zone in the interface crack is specially perceived in the character of the stresses near the crack tip, París *et al.* [102]. Thus, it was stated that for debondings lower than approximately 60°, before appearance of a physically relevant contact zone, normal and tangential stresses showed apparent singular character, in agreement with the open model of interfacial cracks, Toya [137]. But for higher debondings (see for instance the 60° case in fig. 24), in which the appearance of the contact zone is clear), results obtained with the numerical model differ from the analytical solution associated to the open model. The singular behavior of normal stresses along the bonded zone disappears (the values of these normal stresses, in spite of the appearance of a contact zone, for the debonding angle considered, being in tension). The singular behavior of the compression stresses is observed in the incipient contact zone detected. The singular character of the tangential stresses is the same as for lower debondings. For higher debondings, around 80°, the observed tendency for the 60° case is maintained, though normal stresses turn into compressions in the bonded zone.

7.2.3 Energy release rate

The ERR and its components for Modes I and II, obtained with BEM, are represented jointly in fig. 25. Analytical results, associated to the open model, predicted by Toya's solution are also included. An apparently unstable growth up to a maximum of G^{int} placed at the interval between 60° and 70° for the cases studied can be deduced from fig. 25. After the maximum of the curve, there appears a zone of stable growth, where a load increase is necessary for the crack to grow. Mode I decreases when a very small contact zone shows up (near 30° in the present BEM model) and later disappears when the size of the contact zone becomes physically relevant.

The evolution of G^{int}, and its components $G_{\text{I}}^{\text{int}}$ and $G_{\text{II}}^{\text{int}}$, with the debonding permits the appropriateness of using the two interface crack models to be clearly understood. When the debonding is small and no relevant contact zone is detected (SSC conditions), the appropriate model to be used is the open model and the criteria to predict the growth would be those associated to this model, expression (65) in Section 3.2.1. On the other hand, when a relevant contact zone is detected the appropriate model is the Comninou contact model, the growth being controlled by

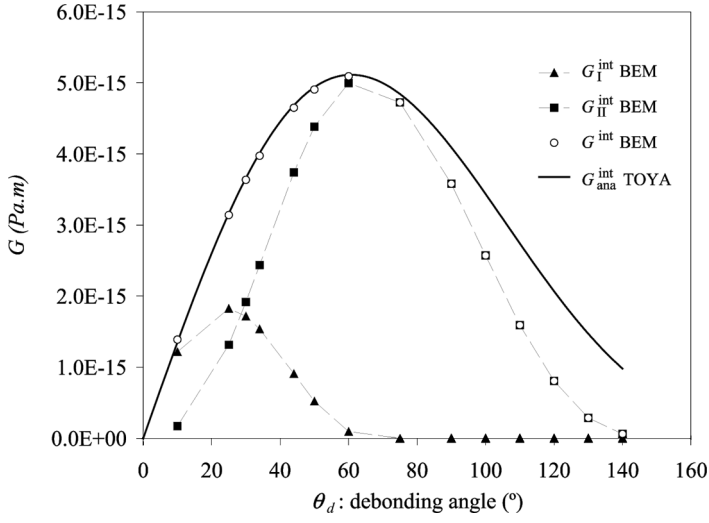

Figure 25: G^{int}, $G_{\text{I}}^{\text{int}}$, $G_{\text{II}}^{\text{int}}$ and $G_{\text{ana}}^{\text{int}}$ for the interface crack.

expression (70), Section 3.2.2. Note the difficulty of establishing the type of growth in the period under SSC conditions ($\theta_d \leq 60^\circ \simeq 70^\circ$) where the open model is applicable. In this interval of debondings the mode mixity is strongly changing and consequently the fracture toughness G_c^{int} is increasing to a great extent in accordance with Section 3.2.1.1. The maximum of this fracture toughness function is the toughness value that controls the growth for greater debondings, $G_c^{\text{int},C}$, where the contact model is applicable.

7.3 Kinking of the interface crack

The study of kinking using BEM can be divided into two different phases: first of all, the determination of the direction of propagation of the kinked crack through the matrix and, secondly, the evaluation of the ERR of the kinked crack along the estimated direction; this parameter will not only allow the character of the growth of the kinked crack to be analyzed, but also would help to decide, by means of a comparison with the ERR of the interface crack, whether the kinking would take place or not at a specified debonding angle.

7.3.1 Orientation of the kinked crack

Referring to the first question, i.e. the search for the expected direction of kinking, maximum circumferential stress (MCS) criterion is applied (see Section 3). Therefore, it is assumed that, if the crack growing along the interface changes its direction of growth to penetrate into the matrix, the chosen direction of growth is that along which the circumferential stress was maximum, based on the fact that Mode I is, in general terms, the main cause of a crack growing and it is along MCS direction that the effect of this mode dominates.

Thus, a numerical study aimed at determining the direction of the MCS at the neighborhood of the crack tip is first performed for two debonding angles $\theta_d = 60^\circ$ and 70°, angles in whose neighborhood it has been found that, as was explained in fig. 25, the stable character of growth of the crack starts.

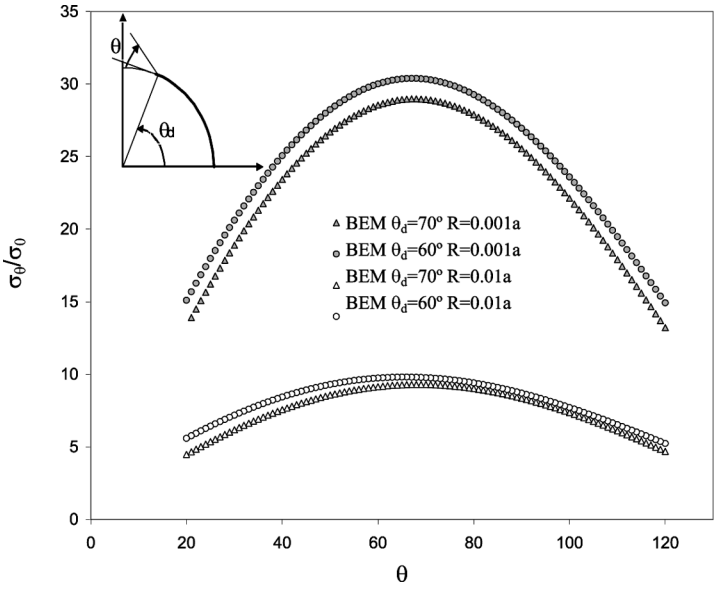

Figure 26: Circumferential stress at the neighborhood of the crack tip.

In the context defined, the value of the circumferential stress along a circumference centred at the crack tip is calculated for different angles of this circumference (fig. 26). The selection of the characteristic distance to the crack tip, referred as radius R at which the study is going to be carried out, must be performed carefully. On one hand the value of R must be small enough in order to allow the possible change of direction of the crack be controlled by the stresses, but on the other hand it must be large enough to maintain the physical meaning of the matrix as a continuum media. Two values of R ($R = 0.1\%$ and 1% of the fiber radius a) satisfying these conditions have been considered.

From the results shown in the fig. 26 it is important to point out that the MCS appear, for the two radii considered, for a value of the circumferential coordinate between 65° and 70°. This direction corresponds to the expected direction, normal to the load, and, moreover, this result can be considered independent of the radius in the range studied. Thus, this conclusion leads us to think that, if kinking occurred, it would not only start in the direction normal to the load, but also the crack growing through the matrix would maintain this direction at least as far as a distance equivalent to the greater value of the radii used, $R = 0.01a$, if no other external factor disturbed crack propagation.

It has to be emphasized that the T-stress term has no noticeable influence in these numerical calculations on the direction of maximum $\sigma_{\theta\theta}$, which supports, at least in this case, the use of MCS criterion based exclusively on the singular term of $\sigma_{\theta\theta}$ stress series expansion.

It is of interest to extend the study carried out for the debondings of 60° and 70° to a wider range of debondings, 25° to 90°, in order to find out whether, for debondings apart from the mechanically expected range of debondings at which kinking occurs, the MCSs also suit the direction normal to the load.

Conclusions obtained from the results of this study can be better understood on the scheme of a fiber fig. 27, where the evolution of the directions of MCS along the fiber-matrix interface has been plotted for the range of θ_d under study. An interval of directions is represented when

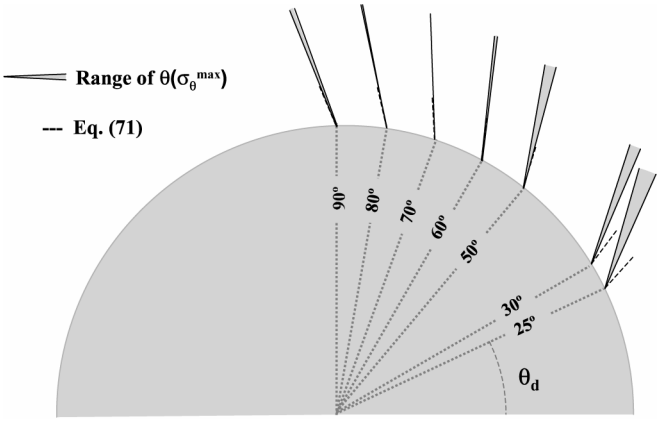

Figure 27: Directions of maximum circumferential stress.

there is a variation in the angle of MCS for different radii R of inspection between $0.01a$ and $0.001a$. The angle predicted by eqn (71) is also represented for comparison. It is possible to observe that the value of this angle is placed in the interval of directions numerically predicted by the MCS criterion for θ_d greater than 50°. This is due to the fact that for these debondings a non negligible contact zone appears at the interface crack tip and the singular asymptotic term of the Comninou contact solution starts to govern the near-tip solution at physically meaningful distances, as $R = 0.01a$ and $R = 0.001a$ considered.

It is clear how the angle of MCS is approximately oriented normal to the nominal load only for values of θ_d in the interval between 60° and 70°, which makes again this interval as the candidate to change the damage from debonding to kinking.

A final interesting point to highlight in the results is that the MCS for each θ_d reaches its maximum as a function of the θ_d between 60° and 70°. Bearing all this in mind it seems logical to think that the value of the debonding angle at which the kinked crack goes into the matrix along the direction of MCS, this direction being normal to the load, is around the interval of $60°-70°$ of θ_d.

7.3.2 Energy release rate at kinking

This section will evaluate how possible it is for a crack that is growing along the interface to go into the matrix following the kinking direction previously determined. To this end an ERR analysis at kinking is going to be performed.

The ERR of a kinked crack associated to a debonding of 70° and penetrating into the matrix along the direction of MCS is now calculated. The results of this case are shown in fig. 28, where ERR values appear, as well as their components, versus the length of the kinked crack.

The unequal contribution of the two modes of failure to the total ERR is first of all noticeable for both cases. While contribution of Mode I, $G_{\mathrm{I}}^{\mathrm{kink}}$, is very important, the contribution of Mode II ERR component, $G_{\mathrm{II}}^{\mathrm{kink}}$, is almost non-existent. This result was foreseeable, observing the completely transversal position of the applied load in relation to the direction of the kinked crack.

Referring to the evolution of the ERR, it can be observed that it increases with the crack length. Thus, taking into account that Mode I completely dominates the growth it can be concluded that crack propagation is unstable. In this situation, once kinked, no additional load increase would be necessary for the crack to continue growing.

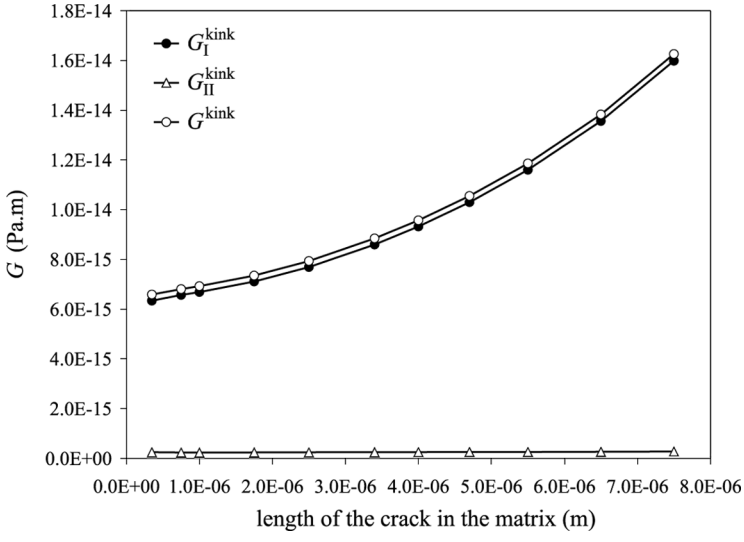

Figure 28: G^{kink}, G_I^{kink} and G_{II}^{kink} for a growing kinked crack for θ_d=70°.

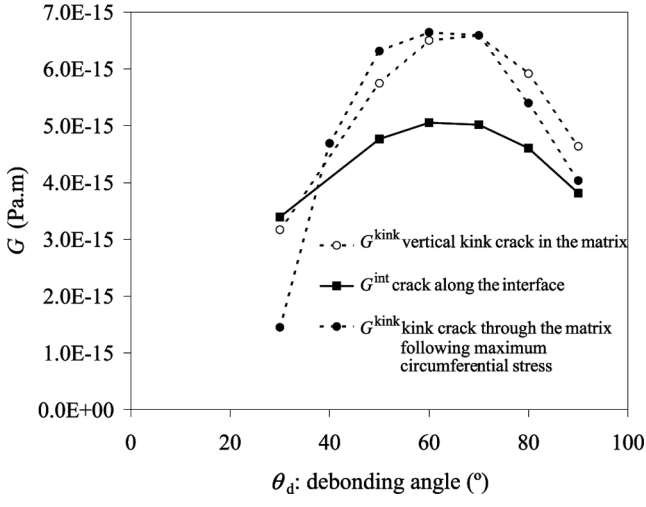

Figure 29: Comparison between ERR of an interface crack and kinked cracks.

Having studied the case of a 70° debonding, the behavior for different debondings is now investigated in order to evaluate the variation with the debonding of the ERR of the kinked crack. Results obtained for debondings in the range under study suit the idea of arising character of the ERR with the length of the kinked crack, previously observed for the 70° case. Minimum values of the curves G^{kink}–θ_d for each debonding in the range under study, that is, nearly asymptotic values of the ERR of the kinked cracks, are represented jointly in fig. 29. The tendency shown in fig. 29 favours the idea that, if kinking appears, the most plausible debonding angles are those between 60° and 70°, where G^{kink} and G_I^{kink} reach a maximum.

In order to have more information about the plausibility of such an occurrence, it is necessary (although not sufficient to conclude whether the kinking appears because, according to (62), it involves the G_c^{int} and G_c^{kink} values of interface and matrix) to compare the ERR of the crack propagating through the matrix, shown in fig. 25, with the ERR of the crack continuing to grow along the interface. Thus, this curve is additionally represented in fig. 29. For the sake of completeness the values of the ERR of a kinked crack growing in the direction of MCS have also been included, in addition to the case of vertical kinked cracks predominantly studied here.

First of all, the two cases of the kinked cracks considered show a coherent evolution with the debonding angle. The values coincide at 70° debonding where the direction of MCS is approximately normal to the nominal load, the values of G at the neighborhood of 70° being very close to each other. The main discrepancies appear for small angles where, in agreement with fig. 27, the MCS direction is quite far from normal direction to the load, the effect of Mode I, which was the dominant contributor to G^{kink}, then being less important.

With reference to the comparison of the ERRs for the kinked crack versus the crack continuing to grow along the interface, the significantly greater values of the ERR of the kinked crack in the interval of interest are quite apparent. It has additionally to be remembered that the presumably unstable growth of the interface crack (after fig. 25) up to a debonding at the neighborhood of $60°-70°$ where the stable growth clearly starts, would theoretically prevent the crack (unless interference with another crack arose) from separating from the interface. At debondings between 60° and 70° the maximum differences appear between the ERR of the crack continuing to grow along the interface and the kink, it having been made clear previously that whereas the growth of the crack along the interface is stable, the growth of the crack penetrating the matrix is unstable.

In addition, and although, as was previously stated, the prediction of growth of the crack along two alternative paths would imply a knowledge of the fracture toughness for the interface and for the matrix, it has to be remembered at this point that whereas the growth along the interface is approximately in Mode II, for larger debonding values, the growth through the matrix is in Mode I, the values of the fracture toughness for Mode I for a determined configuration (material or interface) being significantly smaller than the values of the fracture toughness for Mode II.

All of this supports the idea that the most plausible values of the debondings at which kinking can appear are in the interval between 60° and 70°.

7.4 Concluding remarks

A micromechanical model attempting to represent the real mechanism of matrix failure of a fibrous composite has been developed. First of all, the nature of the contact zone that appears between fiber and matrix has been clarified. This is an important aspect of the problem because the appearance of the contact zone controls the validity of the open model or of the contact model.

When representing the evolution of the ERR with the debonding, it can be seen that the values of the ERR predicted by the open model and the contact model almost coincide until a contact zone of macromechanical meaning appears, which starts to happen for a debonding of 60°. For debondings greater than this, the open model predicts greater values than the contact model (París *et al*. [101]), the correct model to use being the second one.

From a Fracture Mechanics point of view, the evolution of ERR with the debonding angle has shown, for debonding angles greater than those in the interval $60°-70°$, that the energy released is purely in Mode II and the growth of the crack is stable. Comparing this evolution with that of the energy released by a kinked crack for the interval mentioned, the mechanical conditions are favorable for a crack running along the interface to leave it and penetrate into the matrix at a

value of debonding in the interval mentioned, a fact that can be observed experimentally with a reasonable degree of repeatability.

8 Conclusions

A comprehensive review of the present state of knowledge of interfacial fracture mechanics and its applications to composite materials at different levels of modeling have been presented.

The two linear elastic models of interface cracks, open model due to Williams [145] and contact model due to Comninou [19], have been described and reviewed in parallel. A few new theoretical results have been introduced. They may provide a rounded off explanation of the theory available at present. Existing relations between the two models and the adequacy of each model for a particular situation have been discussed in depth.

It is worth mentioning that in the framework of the open model, a new relation between the measures of mixity of fracture Modes I and II based on the SIF approach and on the ERR approach has been deduced. This new and simple relation permits new connections between these two approaches to be generated. In this chapter both approaches have been developed in parallel, self propagation growth of an interface crack and kink appearance together with growth criteria have been revised and the conclusions obtained have been used in the examples shown.

Theoretical fundamentals of the BEM applied to the solution of two-dimensional elastic problems in orthotropic materials have been presented in a concise and modern way using advantages of both, Lekhnitskii and Stroh, complex variable formalisms of two-dimensional elasticity. Orthotropic elastic materials in two-dimensions are classified in two classes depending on the number of different roots of the Lekhnitskii-Stroh characteristic equation of a material, mathematically non-degenerate with different roots and mathematically degenerate with repeated roots of this equation. Explicit and compact formulae of the integral kernels in the Somigliana displacement and stress identities together with the formulae of the coefficient tensor of the free term in the Somigliana displacement identity have been presented for both classes.

An advanced BEM code with the capacity to solve non-linear, friction and frictionless, contact problems has been applied to the analysis of problems in the applications presented. An outstanding feature of this code is its capacity to deal efficiently with non-conforming discretizations of interfaces and contact zones by a weak imposition of the interface and contact conditions. It is also worth mentioning that the removal of the rigid body movements in traction problems is carried out using a procedure based on the Fredholm theory of the boundary integral equations in this code.

The two applications developed have led to several conclusions, some of them deserve to be mentioned.

With reference to the delamination cracks studied in the $[0_m, 90_n]_S$ laminate, it has been found that for a nominal level of load applied, ERR is, from a certain small length of the crack (of a value which is independent of the length of the specimen, and at which Fracture Mechanics at the meso-mechanical level of modeling used is applicable), a constant value and in pure Mode II. This result is in accordance with analytical predictions obtained by means of simplified models.

With reference to the debonding cracks between fiber and matrix the BEM model developed has been used to generate knowledge about the micro-mechanical aspects of the circumferential growth of the crack along the interface and the possibility of its kinking and penetrating into the matrix. In this problem some conclusions derived from the theory developed are applicable. Thus, if the local state of stress predicted by Comninou solution controls the growth of the interfacial crack and its kinking, then the constant relation between the ERR of the interface crack and the ERR of the kinked crack for any debonding implies that as soon as a contact zone of

macro-mechanical meaning appears, the interface crack will kink for this value of the debonding or will not kink for greater debondings. This fact can be quite well observed experimentally.

The knowledge generated in this chapter and in connected publications with the BEM model here presented can constitute the basis for proposing in the future inter-fiber and delamination failure criteria based on the actual mechanism of failure.

References

[1] Amestoy, M., Duong Bui, H. & Dang-Van, K., Deviation infinitésimale d'une fissure dans une direction arbitraire. *C. R. Acad. Sc. Paris*, **289**, 99–102, 1979.

[2] Amestoy, M. & Leblond, J.B., Crack paths in plane situations. II. Detailed form of the expansion of the stress intensity factors. *Int. J. Solids Structures*, **29**, 465–501, 1992.

[3] Anderson, T.L., *Fracture Mechanics: Fundamentals and Applications*, CRC Press: Boca Raton, 1995.

[4] Andersson, T., The boundary element method applied to two-dimensional contact problem with friction. *Boundary Elements Methods*, Springer: Berlin, 239–258, 1982.

[5] Ang, H.E., Torrance, J.E. & Tan, C.L., Boundary element analysis of orthotropic delamination specimens with interface cracks. *Eng. Fract. Mech.*, **54**, 601–615, 1996.

[6] Audoly, B., Asymptotic study of the interfacial crack with friction. *J. Mech. Phys. Solids*, **48**, 1851–1864, 2000.

[7] Avila, R., Mantič, V. & París, F., Application of the boundary element method to elastic orthotropic materials in 2D: Numerical aspects. *Boundary Elements XIX*, eds M. Marchetti, C.A. Brebbia & M.H. Aliabadi, CMP, Southampton, 55–64, 1997.

[8] Banks-Sills, L. & Ashkenazi, D., A note on fracture criteria for interface fracture. *Int. J. Fracture*, **103**, 177–188, 2000.

[9] Bathe, K.J. & Chaudhary, A., A solution method for planar and axisymmetric contact problems. *Int. J. Numer. Meth. Eng.*, **21**, 65–88, 1985.

[10] Blázquez, A., Mantič, V., París, F. & Cañas, J., On the removal of rigid body motions in the solution of elastostatic problems by direct BEM. *Int. J. Numer. Meth. Eng.*, **39**, 4021–4038, 1996.

[11] Blázquez, A., París, F., Cañas, J. & Garrido, J.A., An algorithm for frictionless contact problems with non-conforming discretizations using BEM. *14th International Conference on Boundary Element, BEM XIV*, eds C.A. Brebbia, J. Domínguez & F. París, CMP: Elsevier, 409–420, 1992.

[12] Blázquez, A., París, F. & Cañas, J., Frictional contact problems with non conforming discretizations using BEM. *16th International Conference on Boundary Element, BEM XVI*, ed. C.A. Brebbia, CMP: Southampton, 345–352, 1994.

[13] Blázquez, A. & París, F., Influence of the location of the contact point in node-to-point contact approaches using non-conforming boundary element discretizations. *Contact Mechanics'97. Proc. 3rd Int. Conference*, eds M.H. Aliabadi & A. Samartin, CMP: Southampton, 91–100, 1997.

[14] Blázquez, A., París, F. & Cañas, J., Interpretation of the problems found in applying contact conditions in node-to-point schemes with boundary element non-conforming discretizations. *Eng. Anal. Boundary Elements*, **21**, 361–375, 1998.

[15] Blázquez, A., París, F. & Mantič, V., BEM solution of two-dimensional contact problems by weak application of contact conditions with non-conforming discretizations. *Int. J. Solids Structures*, **35**, 3259–3278, 1998.

[16] Broberg, K.B., On crack paths. *Eng. Fract. Mech.*, **28**, 663–679, 1987.
[17] Broberg, K.B., *Cracks and Fracture*, Academic Press: London, 1999.
[18] Chan, S.K. & Tuba, I.S., A finite element method for contact problems of solid bodies I. Theory and Validation. *Int. J. Mech. Sci.*, **13**, 615–625, 1971.
[19] Comninou, M., The interface crack. *J. Appl. Mech.*, **44**, 631–636, 1977.
[20] Comninou, M., The interface crack with friction in the contact zone. *J. Appl. Mech.*, **44**, 780–781, 1977.
[21] Comninou, M., The interface crack in a shear field. *J. Appl. Mech.*, **45**, 287–290, 1978.
[22] Comninou, M., An overview of interface cracks. *Eng. Fract. Mech.*, **37**, 197–208, 1990.
[23] Comninou, M. & Dundurs, J., Effect of friction on the interface crack loaded in shear. *J. Elasticity*, **10**, 203–212, 1980.
[24] Comninou, M. & Schmueser, D., The interface crack in a combined tension-compression and shear field. *J. Appl. Mech.*, **46**, 345–348, 1979.
[25] Charalambides, M., Kinloch, A.J., Wang, Y. & Williams, J.G., On the analysis of mixed-mode failure. *Int. J. Fracture*, **54**, 269–291, 1992.
[26] Deng, X., General crack-tip fields for stationary and steadily growing interface cracks in anisotropic bimaterials. *J. Appl. Mech.*, **60**, 183–189, 1993.
[27] Deng, X., On stationary and moving interface cracks with frictionless contact in anisotropic bimaterials. *Proc. R. Soc. Lond. A.*, **443**, 563–572, 1993.
[28] Deng, X., An asymptotic analysis of stationary and moving cracks with frictional contact along bimaterial interfaces and in homogeneous solids. *Int. J. Solids Structures*, **31**, 2407–2429, 1994.
[29] Deng, X., A note on interface cracks with and without friction in contact zone. *J. Appl. Mech.*, **61**, 994–995, 1994.
[30] Deng, X., Mechanics of debonding and delamination in composites: asymptotic studies. *Comp. Eng.*, **5**, 1299–1315, 1995.
[31] Dundurs, J., Edge-bonded dissimilar orthogonal elastic wedges under normal and shear loading. *J. Appl. Mech.*, 650–652, 1969.
[32] England, A.H., A crack between dissimilar media. *J. Appl. Mech.*, **32**, 400–402, 1965.
[33] England, A.H., An arc crack around an circular elastic inclusion. *J. Appl. Mech.*, **33**, 637–640, 1966.
[34] Erdogan, F., Stress distribution in bonded dissimilar materials with cracks. *J. Appl. Mech.*, **32**, 403–410, 1965.
[35] Erdogan, F. & Sih, G.C., On the crack extension in plates under plane loading and transverse shear. *J. Basic Eng.*, **85**, 519–527, 1963.
[36] Evans, A.G., Rühle, M., Dalgleish, B.J. & Charalambides, P.G., The fracture energy of bimaterial interfaces. *Metallurgical Transactions A*, **21A**, 2419–2429, 1990.
[37] Foces, A., Garrido, J.A. & París, F., Three-dimensional contact using BEM. *Computational Method in Contact Mechanics*. eds M.H. Aliabadi & C.A. Brebbia, 191–232, 1993.
[38] Fredriksson, B., Finite element solution of surface nonlinearities in structural mechanics with special emphasis to contact and fracture mechanics problems. *Comput. & Struct.*, **6**, 281–290, 1976.
[39] Garrido, J.A., Foces, A. & París, F., B.E.M. applied to receding contact problems with friction. *Math. Comput. Modell.*, **15**, 143–154, 1991.
[40] Gautesen, A.K. & Dundurs, J., The interface crack in a tension field. *J. Appl. Mech.*, **54**, 93–98, 1987.
[41] Gautesen, A.K. & Dundurs, J., The interface crack under combined loading. *J. Appl. Mech.*, **55**, 580–586, 1988.

[42] Gerberich, W. & Yang, W., (eds). Interfacial and Nanoscale Failure (Vol. 8). *Comprehensive Structural Integrity*, Editors-in-Chief I. Milne, R.O. Ritchie & B. Karihaloo, Elsevier Pergamon: Amsterdam, 2003.
[43] Geubelle, P.H. & Knauss, W.G., Crack propagation at and near bimaterial interfaces: linear analysis 1. *J. Appl. Mech.*, **61**, 560–566, 1994.
[44] Geubelle, P.H. & Knauss, W.G., Crack propagation in homogeneous and bimaterial sheets under general in-plane loading: nonlinear analysis. *J. Appl. Mech.*, **62**, 601–606, 1995.
[45] Gladwell, G.M.L., *Contact Problems in the Classical Theory of Elasticity*, Sijthoff and Nordhoff, 1980.
[46] Goldstein, R.V. & Salganik, R.L., Brittle fracture of solids with arbitrary cracks. *Int. J. Fract.*, **10**, 5047–523, 1974.
[47] Graciani, E., París, F. & Mantič, V., Single fiber fragmentation test. A BEM analysis. *44th AIAA/ASME/ASCE/AHS Structure Dynamics, and Materials Conference*, Norfolk: Virginia, 2003.
[48] Hayashi, K. & Nemat-Nasser, S., Energy release rate and crack kinking under combined loading. *J. Appl. Mech.*, **48**, 520–524, 1981.
[49] Hayashi, K. & Nemat-Nasser, S., On branched, interface cracks. *J. Appl. Mech.*, **48**, 529–533, 1981.
[50] He, M-Y. & Hutchinson, J.W., Kinking of a crack out of an interface. *J. Appl. Mech.*, **56**, 270–278, 1989.
[51] He, M-Y., Barlett, A., Evans, A.G. & Hutchinson, J.W., Kinking of a crack out of an interface: role of in-plane stress. *J. Am. Ceram. Soc.*, **74**, 767–771, 1991.
[52] Hertz, H., *Miscellaneous papers on the contact of elastic solids*, Translation by Jones, D.E. McMillan: London, 1896.
[53] Hills, D.A. & Barber, J.R., Interface cracks. *Int. J. Mech. Sci.*, **35**, 27–37, 1993.
[54] Hills, D.A., Kelly, P.A., Dai, D.N. & Korsunsky, A.M., *Solutions of Crack Problems. The Distributed Dislocation Technique*, Kluwer Academic Publishers: Dordrecht, 1996.
[55] Huesmann, A. & Kuhn, G., Non-conform discretisation of the contact region applied to two-dimensional Boundary Element Method, *Boundary Elem. Meth. XVI*, ed. C.A. Brebbia, 353–360, 1994.
[56] Hutchinson, J.W. & Suo, Z., Mixed mode cracking in layered materials. *Advances in Applied Mechanics*, (Editors-in-Chief) J.W. Hutchinson & T.Y. Wu, Academic Press: New York, **29**, 63–191, 1992.
[57] Hwu, C., Fracture parameters for the orthotropic bimaterial interface cracks, *Eng. Fract. Mech.*, **45**, 89–97, 1993.
[58] Hwu, C. & Hu, J.S., Stress intensity factors and energy release rates of delaminations in composite laminates. *Eng. Fract. Mech.*, **42**, 977–988, 1992.
[59] Irwin, G.R., Analysis of stresses and strains near the end of a crack traversing a plate. *J. App. Mech.*, **24**, 361–364, 1957.
[60] Janssen, M., Zuidema, J. & Wanhill, R.J.H., *Fracture Mechanics*, Delft University Press, 2002.
[61] Johnson, K.L., *Contact Mechanics*, Cambridge University Press: Cambridge (U.K.), 1985.
[62] Klarbring, A & Björkman, G., Solution of large displacement contact problems with friction using Newton's method for generalized equations. *Int. J. Numer. Meth. Eng.*, **34**, 249–269, 1992.
[63] Knowles, J.K. & Sternberg, E., Large deformations near the tip of an interface crack between two Neo-Hookean sheets. *J. Elasticity*, **13**, 257–293, 1983.

[64] Leblond, J.B. & Mourd, P., Crack Propagation from a Preexisting Flaw at a Notch Root. *C.R. Acad. Sci. Paris*, **327**, Série IIb, 581–587, 1999.
[65] Leblond, J.B. & Frelat, J., Crack kinking form an initially closed interface crack. *C. R. Acad. Sci. Paris*, **327**, 1311–1318, 1999.
[66] Leblond, J.B. & Frelat, J., Crack kinking form an interface crack with initial contact between the crack lips. *Eur. J. Mech. A/Solids*, **20**, 937–951, 2001.
[67] Leblond, J.B. & Frelat, J., Crack kinking form an initially closed interface crack, ordinary or interface crack, in the presence of friction. *Eng. Fract. Mech.*, **71**, 289–307, 2004.
[68] Lee, J. & Gao, H., A generalized Comninou contact model for interface cracks in anisotropic elastic solids. *Int. J. Fract. Mech.*, **67**, 53–68, 1994.
[69] Lee, K.Y. & Choi, H.J., Boundary element analysis of stress intensity factors for bimaterial interface cracks. *Eng. Fract. Mech.*, **29**, 461–472, 1988.
[70] Leguillon, D., Interface crack tip singularity with contact and friction. *C. R. Acad. Sci. Paris*, **327**, 437–442, 1999.
[71] Lekhnitskii, S.G., Some cases of the elastic equilibrium of a homogeneous cylinder with arbitrary anisotropy, *Applied Mathematics and Mechanics (in Russian)*, **2**, 345–367, 1938.
[72] Liechti, K.M. & Chai, Y.S., Biaxial loading experiments for determinating interfacial fracture toughness. *J. Appl. Mech.*, **58**, 680–687, 1991.
[73] Liechti, K.M. & Chai, Y.S., Asymmetric shielding in interfacial fracture under in-plne shear. *J. Appl. Mech.*, **59**, 295–304, 1992.
[74] Liu, C.H. & Feng-Chen, I., Interface cracks in a layered solid subjected to contact stresses. *J. Appl. Mech.*, **63**, 271–277, 1996.
[75] Malyshev, B.M. & Salganik, R.L., The strength of adhesive joints using the theory of cracks. *Int. J. Fract. Mech.*, **1**, 114–128, 1965.
[76] Man, K.W., Aliabadi, M.H. & Rooke, D.P., BEM frictional contact analysis: modelling considerations, *Eng. Anal. Boundary Elements*, **11**, 77–85, 1993.
[77] Mantič, V., Blázquez, A., París, F. & McCartney, N.L., Analysis of delamination cracks in 0/90 symmetric laminates by BEM. *IABEM 2002* (CD), International Association for Boundary Element Methods, The University of Texas at Austin, USA, 2002.
[78] Mantič, V. & París, F., Explicit formulae of the integral kernels and C-matrix in the 2D Somigliana identity for orthotropic materials. *Eng. Anal. Boundary Elements*, **15**, 283–288, 1995.
[79] Mantič, V. & París, F., On Stroh orthogonality relations: an alternative proof applicable to Lekhnitskii and Eshelby theories of an anisotropic body. *J. Elasticity*, **43**, 137–145, 1996.
[80] Mantič, V. & París, F., Symmetrical representation of stresses in the Stroh formalism and its application to a dislocation and a dislocation dipole in an anisotropic elastic medium. *J. Elasticity*, **47**, 101–120, 1997.
[81] Mantič, V. & París, F., Integral kernels in the 2D Somigliana displacement and stress identities for anisotropic materials. *Comp. Mech*, **22**, 77–87, 1998.
[82] Mantič, V. & París, F., Relation between SIF and ERR based measures of fracture mode mixity in interface cracks. *Int. J. Fracture*, **130**, 557–569, 2004.
[83] Matsumoto, T., Tanaka, M. & Obara, R., Computation of stress intensity factors of interface cracks based on interaction energy release rates and BEM sensitivity analysis. *Eng. Fract. Mech.*, **65**, 683–702, 2000.
[84] Melin, S., Fracture from a straight crack subjected to mixed mode loading. *Int. J. Fract.*, **32**, 257–263, 1987.
[85] Melin, S., Growth from a straight crack subjected to arbitrary remote loading. *Eng. Fract. Mech.*, **46**, 511–518, 1993.

[86] Melin, S., Accurate data for stress intensity factors at infinitesimal kinks. *J. Appl. Mech.*, **61**, 467–470, 1994.
[87] Miller, G.R. & McDowell, D.L., *Mixed-mode crack behaviour, ASTM STP 1359*, American Society for Testing and Materials, West Conshohocken, PA, 1999.
[88] Miller, G.R. & Stock, W.L., Analysis of branched interface cracks between dissimilar anisotropic media. *J. Appl. Mech.*, **56**, 844–849, 1989.
[89] Mukai, D.J., Ballarini, R. & Miller, G.R., Analysis of branched interface cracks. *J. Appl. Mech.*, **57**, 887–893, 1990.
[90] Muskhelishvili, N.I., *Some Basic Problems of the Mathematical Theory of Elasticity*, Nordhoff International Publishing, 1962.
[91] O'Brien, T.K., Analysis of local delaminations and their influence on composite laminate behavior. *Delamination and Debonding of Materials, ASTM STP 876*, ed. W.S. Johnson, American Society for Testing and Materials, Philadelphia, 282–297, 1985.
[92] Oden, J.T. & Pires, E.B., Algorithms and numerical results for finite element approximations of contact problems with non-classical friction laws. *Comput.& Struct.*, **19**, 137–147, 1984.
[93] Okamoto, N. & Nakazawa, M., Finite element incremental contact analysis with various frictional conditions. *Int. J. Numer. Meth. Eng.*, **14**, 337–357, 1979.
[94] Olukoko, O.A., Becker, A.A. & Fenner, R.T., A new boundary element approach for contact problems with friction. *Int. J. Numer. Meth. Eng.*, **36**, 2625–2642, 1993.
[95] París, F., *A Study of Failure Criteria of Fibrous Composite Materials*, NASA/CR-2001–210661, 2001.
[96] París, F. & Blázquez, A., On the displacement and load scaling techniques in contact problems using BEM. *Boundary Elements Communications*, **5**, 15–17, 1994.
[97] París, F., Blázquez, A. & Cañas, J., Contact problems with non-conforming discretizations using boundary element method. *Comput. & Struct.*, **57**, 829–839, 1995.
[98] París, F., Blázquez, A., Cañas, J. & Mantič V., A comparison between non-conforming node-to-point and weak approaches in contact problem by BEM. *20th Int. Conf. in Boundary Elements, Advances in Boundary Elements*, eds, A. Kassab, M. Chopra & C.A. Brebbia, CMP: Southampton, 117–126, 1998.
[99] París, F., Blázquez, A., Mantič, V. & McCartney, N.L., Caracterización de grietas de delaminación en laminados 0–90 simétricos. *Materiales Compuestos 01*, AEMAC, Gijón, Spain, 241–248, 2001.
[100] París, F. & Cañas, J., *Boundary Element Method. Fundamentals and Applications*, Oxford University Press, 1997.
[101] París, F., del Caño, J.C. & Varna, J., The fibre-matrix interface crack- A numerical analysis using Boundary Elements. *Int. J. Fracture*, **82**, 11–29, 1996.
[102] París, F., Correa, E. & Cañas, J., Micromechanical view of failure of the matrix in fibrous composite materials. *Comp. Sci. & Tech.*, **63**, 1041–1052, 2003.
[103] París, F., Correa, E. & Mantič, V., Micromechanical bases for the prediction of failure in Fibrous Composites. *44th AIAA/ASME/ASCE/AHS Structure Dynamics, and Materials Conference*, Norfolk: Virginia, 2003.
[104] París, F. & Garrido, J.A., On the use of discontinuous elements in two dimensional contact problems. *Boundary Elements VII*, eds Brebbia & Maier, Springer: Berlin, **2**, 1327–1330, 1985.
[105] París, F & Garrido, J.A., Friction multicontact problems with BEM. *Boundary Elements X*, Proc. 10th Int. Conference, ed. C.A. Brebbia, CMP: Southampton, 1988.

[106] París, F. & Garrido, J.A., An incremental procedure for friction contact problems. *Eng. Anal. Boundary Elements*, **6**, 202–213, 1989.
[107] París F., Garrido, J.A. & Foces A., An incremental procedure for three-dimensional contact problems with friction, *Comput. & Struct.*, **50**, 201–215, 1994.
[108] Paula de, F.A. & Aliabadi, M.H., Boundary element analysis of interface cracks in dissimilar orthotropic materials using a path independent contour integral. *Boundary Elements XIX*, eds M. Marchetti, C.A. Brebbia, & M.H. Aliabadi, Computational Mechanics Publications: Southampton, 359–366, 1997.
[109] Pook, L.P., *Crack Paths*, WIT Press: Southampton, 2002.
[110] Qian, W. & Sun, S.T., A frictional interfacial crack under combined shear and compression. *Comp. Sci. & Tech.*, **58**, 1753–1761, 1998.
[111] Raju, I.S., Crews, J.H. & Aminpour, M.A., Convergence of strain energy release rate components for edge-delaminated composite laminates. *Eng. Fract. Mech.*, **30**, 383–396, 1988.
[112] Rice, J.R., Elastic fracture mechanics concepts for interfacial cracks. *J. Appl. Mech.*, **55**, 98–103, 1988.
[113] Rice, J.R. & Sih, G.C., Plane problems of cracks in dissimilar media. *J. Appl. Mech.*, **32**, 418–423, 1965.
[114] Rice, J.R., Suo, Z. & Wang, J.S., Mechanics and thermodynamics of brittle interfacial failure in bimaterial systems. *Metal-Ceramics Interfaces*, eds, M. Rühle, A.G. Evans, M.F. Ashby & J.P. Hirth, Pergamon: New York, 269–294, 1990.
[115] Selcuk, S., Hurd, D.S., Crouch, S.L. & Gerberich, W.W., Prediction of interfacial crack path: a direct boundary integral approach and experimental study. *Int. J. Fracture*, **67**, 1–20, 1994.
[116] Shield, R.T., Uniqueness for elastic crack and punch problems. *J. Appl. Mech.*, **49**, 516–518, 1982.
[117] Shih, C.F. & Asaro, R.J., Elastic-plastic analysis of cracks on bimaterial interfaces: Part I-Small scale yielding. *J. Appl. Mech.*, **55**, 299–316, 1988.
[118] Shih, C.F. & Asaro, R.J., Elastic-plastic analysis of cracks on bimaterial interfaces: Part II-Structure of small scale yielding fields. *J. Appl. Mech.*, **56**, 763–779, 1989.
[119] Sih, G.C., Paris, P.C. & Irwin, G.R., On cracks in rectilinear anisotropic bodies. *Int. J. Fract. Mech.*, **1**, 189–302, 1965.
[120] Sládek J. & Sládek V., Evaluations of the T-stress for interface cracks by the boundary element method. *Eng. Fract. Mech.*, **56**, 813–825, 1997.
[121] Stringfellow, R.G. & Freund, L.B., The effect of interfacial friction on the buckle-driven spontaneous delamination of a compressed thin film. *Int. J. Solids Structures*, **30**, 1379–1395, 1993.
[122] Stroh, A.N., Dislocations and cracks in anisotropic elasticity. *Phil. Mag*, **3**, 625–646, 1958.
[123] Stroh, A.N., Steady state problems in anisotropic elasticity. *J. Math. Phys.*, **41**, 77–103, 1962.
[124] Sun, S.T. & Jih, C.J., On strain energy release rates for interfacial cracks in bi-material media. *Eng. Fract. Mech.*, **28**, 13–20, 1987.
[125] Sun, S.T. & Qian, W., The use of finite extension strain energy release rates in fracture of interfacial cracks. *Int. J. Solids Structures*, **34**, 2595–2609, 1997.
[126] Sun, S.T. & Qian, W., A treatment of interfacial cracks in the presence of friction. *Int. J. Fract.*, **94**, 371–382, 1998.
[127] Suo, Z., Singularities, interfaces and cracks in dissimilar anisotropic media. *Proc. R. Soc. Lond. A.*, **427**, 331–358, 1990.

[128] Swadener, J.G. & Liechti, K.M., Asymmetric shielding mechanisms in the mixed-mode fracture of a glass/epoxy interface. *J. Appl. Mech.*, **65**, 25–29, 1998.
[129] Swadener, J.G., Liechti, K.M. & de Lozanne, A.L., The intrinsic toughness and adhesion mechanisms of a glass/epoxy interface. *J. Mech. Phys. Solids*, **47**, 223–258, 1999.
[130] Tan, C.L., Gao, Y.L. & Afagh, F.F., Boundary element analysis of interface cracks between dissimilar anisotropic materials. *Int. J. Solids Structures*, **29**, 3201–3220, 1992.
[131] Tewary, V.K. & Kriz, R.D., Generalized Plane Strain Analysis of Bimaterial Composite a Free Surface Normal to the Interface. *J. Material Research*, **13**, 2609–2622, 1991.
[132] Ting, T.C.T., *Anisotropic Elasticity, Theory and Applications*, Oxford University Press, Oxford, 1996.
[133] Ting, T.C.T., Explicit solution and invariance of the singularities at an interface crack in anisotropic composites. *Int. J. Solids and Structures*, **22**, 965–983, 1986.
[134] Ting, T.C.T. & Hoang, P.H., Singularities at the tip of a crack normal to the interface of an anisotropic layered composite. *Int. J. of Solids and Structures*, **20**, 439–454, 1984.
[135] Tvergaard, V., Resistance curves for mixed mode interface crack growth between dissimilar elasti-plastic solids. *J. Mech. Phys. Solids*, **49**, 2689–2703, 2001.
[136] Tvergaard, V. & Hutchinson, J.W., The influence of plasticity on mixed mode interface toughness. *J. Mech. Phys. Solids*, **41**, 1119–1135, 1993.
[137] Toya, M., The interface crack. *J. Mech. Phys. Solids*, **22**, 325–348, 1975.
[138] Toya, M., On mode I and mode II energy release rates of an interface crack. *Int. J. Fracture*, **56**, 345–352, 1992.
[139] Vaughan, H., Crack propagation and the principal-tensile-stress criterion for mixed-mode loading. *Eng. Fract. Mech.*, **59**, 393–397, 1998.
[140] Volinsky, A.A., Nanoindentation methods in interfacial fracture testing. *Comprehensive Structural Integrity, Vol. 8: Interfacial and Nano Scale Failure*, Volume Editors W. Gerberich & W. Yang, Editors-in-Chief I. Milne, R.O. Ritchie & B. Karihaloo, Elsevier Pergamon, 2003.
[141] Wang, C.H., Fracture of interface cracks under combined loading. *Eng. Fract. Mech.*, **56**, 77–86, 1997.
[142] Wang, T.C., Kinking of an interface crack between two dissimilar anisotropic elastic solids. *Int. J. Solids Structures*, **31**, 629–641, 1994.
[143] Wang, T.C., Shih, C.F. & Suo, Z., Crack extension and kinking in laminates and bicrystals. *Int. J. Solids Structures*, **29**, 327–344, 1992.
[144] Wang, J.S. & Suo, Z., Experimental determination of interfacial toughness curves using brazil-nut sandwiches. *Acta Metall. Mater.*, **38**, 1279–1290, 1990.
[145] Williams, M.L., The stress around a fault of crack in dissimilar media. *Bull. Seismol. Soc. Am.*, **49**, 199–204, 1959.
[146] Wu, K.C., Stress intensity factor and energy release rate for interfacial cracks between dissimilar anisotropic materials. *J. Appl. Mech.*, **57**, 882–886, 1990.
[147] Wu, K.C., Correspondence relations for the interface crack in monoclinic composites under mixed loading. *J. Appl. Mech.*, **57**, 894–900, 1990.
[148] Wu, K.C., Explicit crack-tip fields of an extending interface crack in an anisotropic bimaterial. *Int. J. Solids Structures*, **27**, 455–466, 1991.
[149] Wu, K.C., On the contact zone model for interface cracks in anisotropic bimaterials. *J. Appl. Mech.*, **58**, 399–403, 1992.
[150] Yuuki, R. & Cho, S.-B., Efficient boundary element analysis of stress intensity factors for interface cracks in dissimilar materials. *Eng. Fract. Mech.*, **34**, 179–188, 1989.
[151] Yuuki, R., Liu, J.Q., Xu, J.Q., Ohira, T. & Tomoyoshi, O., Mixed mode fracture criteria for an interface crack. *Eng. Fract. Mech.*, **47**, 367–377, 1994.